nature immunology

Article

https://doi.org/10.1038/s41590-026-02481-y

Blood vessel-resident macrophages safeguard blood and vessel integrity in zebrafish

Received: 22 September 2025

Accepted: 26 February 2026

Published online: 31 March 2026

Check for updates

Bart Weijts[1] ✉, Jeroen A. A. Demmers[2] & Catherine Robin[1,3] ✉

Tissue-resident macrophages populate nearly all organs, where they adopt tissue-specific roles essential for immune defense, tissue development and homeostasis. Their dysfunction contributes to inflammation, cancer and other diseases. Whether a dedicated macrophage population operates within the extensive vascular network, one of the body's largest and most widely distributed tissues, has remained unknown. Here, using high-resolution spatiotemporal live imaging in zebrafish embryos, we identify a distinct population of macrophages residing within blood vessels, termed blood vessel-resident macrophages (bMΦs), with conserved features in mice. bMΦs patrol the bloodstream, clear foreign particles and unfit cells, and act as first responders to endothelial damage. bMΦs emerge directly from axial vessels through an atypical endothelial-to-macrophage transition that is independent of Runx1 and Csf1r. Our findings reveal a previously unrecognized macrophage population dedicated to vascular immune surveillance, uncovering mechanisms that preserve blood and vessel integrity and offering potential therapeutic avenues for bloodborne and vascular diseases.

Macrophages, first described over a century ago for their ability to engulf debris and pathogens, display remarkable plasticity and heterogeneity[1–3]. Present in nearly all tissues from early fetal development through adult life, most tissue-resident macrophages originate from yolk-sac-derived erythroid–myeloid progenitors (EMPs), with partial replacement by macrophages originating from bone marrow hematopoietic stem cell-derived monocytes[4–7]. Given the scale of the vertebrate vascular network and the need to maintain blood quality and endothelial integrity, it remains unclear whether a dedicated macrophage population resides inside blood vessels. Kupffer cells in hepatic sinusoids filter portal venous blood to remove gut-derived microbes and debris[8], and red pulp macrophages phagocytose senescent erythrocytes and pathogens within the unique open circulatory system of the spleen[9,10]. However, these actions are restricted to these tissues' specific vascular niches, leaving most blood vessels unmonitored. Patrolling monocytes can initiate early immune responses[11], yet rapidly extravasate into the infected tissue and differentiate into macrophages[11], emphasizing their transient nature. Here, we identify a bona fide population of intravascular macrophages that continuously safeguards blood and vessel integrity, which we term blood vessel-resident macrophages (bMΦs).

To determine how threats are cleared from the bloodstream, fluorescently labeled foreign particles and cells were injected into the circulation of zebrafish embryos 3 days post fertilization (dpf), in which the *fli1a* promoter drives mCherry expression and labels all vascular endothelial cells (ECs)[12] (Fig. 1a). Within 30 min, particles and cells were exclusively phagocytosed by cells with an unusually bright mCherry signal (mCherry^{bright}) (Fig. 1b, Extended Data Fig. 1a and Supplementary Video 1). These phagocytic mCherry^{bright} cells were located inside venous blood vessels of the caudal part of the trunk, also

[1]Hubrecht Institute-KNAW, University Medical Center Utrecht, Utrecht, the Netherlands. [2]Proteomics Center, Erasmus University Medical Center, Rotterdam, the Netherlands. [3]Regenerative Medicine Center, University Medical Center Utrecht, Utrecht, the Netherlands. ✉e-mail: b.weijts@hubrecht.eu; c.robin@hubrecht.eu

known as the caudal vein plexus (CVP). Under homeostatic conditions, mCherry^{bright} cells were already present in the CVP and their numbers did not change after foreign particle exposure (Fig. 1b, bottom, and Extended Data Fig. 1b). Zymosan injected into the tissue adjacent to the CVP did not result in extravasation of intravascular mCherry^{bright} cells (Fig. 1c and Supplementary Video 2), indicating that they function within the vasculature. High-spatiotemporal-resolution imaging showed that mCherry^{bright} cells were not embedded in vessel walls but crawled with an ameboid-like movement along the luminal surface, independently of blood flow direction (Fig. 1d and Supplementary Videos 3 and 4), often transiently obstructing flow, indicative of strong endothelial adhesion (Supplementary Video 4).

To identify the nature of mCherry^{bright} cells, we crossed our fli1a reporter line with the reporter transgenic lines *Tg(mpx:GFP)*[13] (where Tg is transgenic, *mpx* is myeloid-specific peroxidase and GFP is green fluorescent protein) and *Tg(mpeg:GFP)*[14] (where *mpeg* is macrophage expressed 1 (tandem duplicate 1; mpeg1.1)), which label neutrophils and macrophages, respectively. While no mCherry^{bright} cells expressed GFP in the neutrophil line (Fig. 2a, top), they all expressed GFP in the macrophage line (Fig. 2a, bottom), indicating a macrophage identity. mCherry^{bright} cells were also detected using combinations of alternative endothelial specific (that is, *kdrl* and *flt4*)[15,16] and macrophage (mpeg)[17] reporter line (Extended Data Fig. 2a–g). We thus identified a population of phagocytic macrophages expressing endothelial markers and confined to the vasculature, which we termed blood vessel-resident macrophages (bMΦs).

We then sorted bMΦs (fli1a$^+$mpeg$^+$), macrophages residing within the tissue (fli1a$^-$mpeg$^+$, referred to as tissue macrophages), ECs (fli1a$^+$mpeg$^-$) and neutrophils (mpx$^+$) on the basis of fluorescent reporter expression to compare their morphology. bMΦs were distinguishable by filopodia-like protrusions on their surface (Fig. 2b and Extended Data Fig. 2h,i). Such actin-rich protrusions are typically used for attachment, migration, and as cellular tentacles to sense, catch and pull particles[18,19]. Inhibition of actin polymerization by a low dose of Latrunculin A impaired bMΦ attachment (Fig. 2c and Supplementary Video 5) and reduced clearance of intravascularly injected zymosan, leaving most particles circulating freely (Fig. 2d, arrows). These protrusions are therefore essential for endothelial adhesion and phagocytosis. Intravascular injection of fluorescently labeled peanut agglutinin (PNA) did not bind to bMΦs, but only to CVP venous ECs (Extended Data Fig. 2j), demonstrating that bMΦs are not dendritic cells (DCs), which also display similar filopodia-like protrusions or dendrites[20,21]. Altogether, we identified a previously unrecognized population of intravascular macrophages, marked by endothelial (*fli1a, kdrl* and *flt4*) and macrophage (*mpeg*) reporters, that actively phagocytoses foreign particles and cells within the bloodstream.

Macrophage development depends on spi-1 proto-oncogene b (*spi1b*) (*PU.1*)[22] and downstream-acting interferon regulatory factor 8 (*irf8*)[23]. While *spi1b* is required for the differentiation of EMPs into bipotential neutrophil–macrophage progenitors[22], *irf8* skews these progenitors toward macrophage lineage at the expense of neutrophils[24,25]. Injection of well-characterized morpholino oligonucleotides (MOs) to knock down *irf8*[25] or *spi1b*[22] eliminated nearly all bMΦs and tissue macrophages (Fig. 2e), indicating that bMΦ formation relies on classical myeloid transcription factors. Accordingly, zymosan injected into the circulation of *spi1b* morphants was not phagocytosed (Fig. 2f and Supplementary Video 6), confirming that bMΦs are solely responsible for clearing foreign particles from the blood. We next analyzed blood from *Tg(fli1a:laCherry; mpeg:GFP)* (where laCherry is lifeactCherry) adult zebrafish and identified laCherry$^+$GFP$^+$ cells resembling embryonic bMΦs (Fig. 2g,h), which phagocytosed retro-orbitally injected zymosan into *Tg(fli1a:laCherry)* adults (Fig. 2i). Thus, bMΦs are also present and functionally active in adult zebrafish.

We then asked whether bMΦs contribute to blood homeostasis, for example by monitoring endogenous circulating cells. bMΦs can be uniquely identified by their distinct mCherry^{bright} appearance, allowing the use of GFP reporter lines to mark erythrocytes or hematopoietic stem and progenitor cells (HSPCs). High-temporal single *z*-plane imaging of the CVP region showed bMΦs (mCherry^{bright}) catching circulating erythrocytes (GFP$^+$) and, after prolonged surface interactions, either releasing them (Fig. 3a and Supplementary Video 7) or phagocytosing them (Fig. 3b and Supplementary Videos 8 and 9). Phagocytosed erythrocytes were often unusually large, suggesting that bMΦs eliminate abnormal or unfit cells from the circulation. Importantly, this surveillance behavior was not restricted to erythrocytes but extended also to HSPCs (Fig. 3c and Supplementary Video 10), with occasional uptake of a small portion of fluorescent cytoplasmic material through trogocytosis (Fig. 3d), release or phagocytosis (Fig. 3e).

To further explore bMΦ function in tissue homeostasis, we adapted an ultraviolet (UV) light-responsive optogenetic tool[26] to induce EC apoptosis (Fig. 3f, top). We ablated ECs in a single intersegmental vessel (ISV) in embryos expressing the transgene *PhoCl2c-Bid-mClover* (where Bid is BH3 interacting-domain death agonist), either stably in all ECs or mosaically. In these embryos, bMΦs (fli1a$^+$mpeg$^+$) rapidly arrived at the injury site, efficiently clearing EC debris (fli1a$^+$mpeg$^-$) while neighboring tissue macrophages (fli1a$^-$mpeg$^+$) dwelled only shortly around the injury site and occasionally phagocytosed EC debris (Fig. 3f, bottom, asterisks, Extended Data Fig. 3a and Supplementary Videos 11 and 12). Neutrophils are known for their rapid response to damage. However, like tissue macrophages, neutrophils were only occasionally recruited, had short dwell times around the injury and showed little to no phagocytosis of EC debris (Extended Data Fig. 3b, arrows, and Supplementary Video 13). Altogether, these data suggest that bMΦs contribute to blood and vascular homeostasis by surveying the circulation for foreign particles and unfit endogenous cells and by serving as first responders to EC damage.

To study the spatiotemporal origin of bMΦs, we imaged the entire trunk region starting from ~20 hpf. Just after the initiation of blood flow (~25 hpf), bMΦs (visualized as mCherry^{bright}) emerged from both the roof and floor of the dorsal aorta (DA) and from the roof of the posterior cardinal vein (PCV) (Fig. 4a). Although bMΦs were also produced from the PCV floor, their emergence was difficult to image owing to delayed mCherry expression at this time point[27]. After emergence, bMΦs entered the bloodstream; some appeared in the common cardinal vein (CCV), which runs bilaterally over the yolk ball, while others traveled to the caudal vein (Fig. 4a,

Fig. 1 | Intravascular fli1a mCherry^{bright} cells phagocytose foreign particles and cells. a, Schematic representation of a 3-dpf zebrafish embryo. The axial view (dashed box) is generated postprocessing to visualize the intraluminal space of the blood vessels. Anterior is oriented to the left for all imaging data in this study. **b**, Images of the CVP of 3-dpf *Tg(fli1a:laCherry)* embryos after intravascular injection of fluorescently labeled particles (*E. coli*, zymosan (*S. cerevisiae* bioparticles), polymeric beads) or cells (donor erythrocytes from adult *Tg(globin:eGFP)*) (green). Injection in the CCV as indicated in the scheme in **a**. All ECs (*fli1a*) are labeled with laCherry (magenta) that is fused N-terminally to lifeact (la), a small actin-binding peptide that is incorporated into the actin cytoskeleton. GFP$^+$ particles and cells (green) were exclusively phagocytosed by mCherry^{bright} cells. The bottom panel shows the non-injected control. mCherry^{bright} cells are indicated by asterisks. **c**, Still images of Supplementary Video 2 in which zymosan particles (green) were injected into the tissue adjacent to the CVP of a *Tg(fli1a:laCherry)* embryo. **d**, Still images of Supplementary Videos 3 (left) and 4 (right), showing 3-dpf *Tg(fli1a:laCherry)* embryos injected with zymosan (left) or not injected (right). DA, CVP, erythrocytes and mCherry^{bright} cells are outlined and colored on brightfield single *z*-slide images. Images are representative of $n = 3$ independent experiments (30 embryos analyzed in total) (**b**), $n = 2$ (10 embryos analyzed in total) (**c**), and 2 and 5 independent time-lapse experiments, respectively (**d**). Scale bars, 20 µm. e, erythrocyte.

https://doi.org/10.1038/s41590-026-02481-y

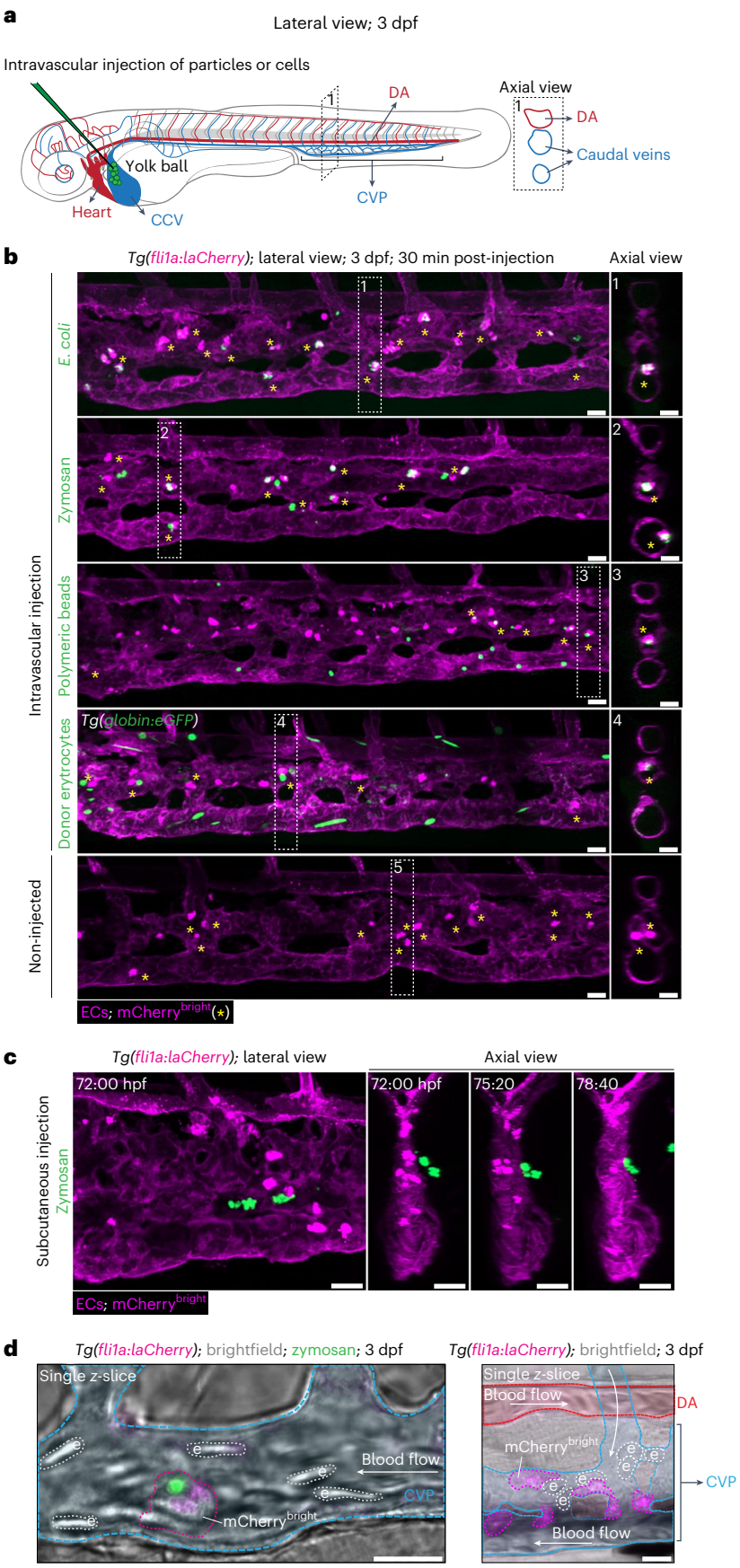

https://doi.org/10.1038/s41590-026-02481-y

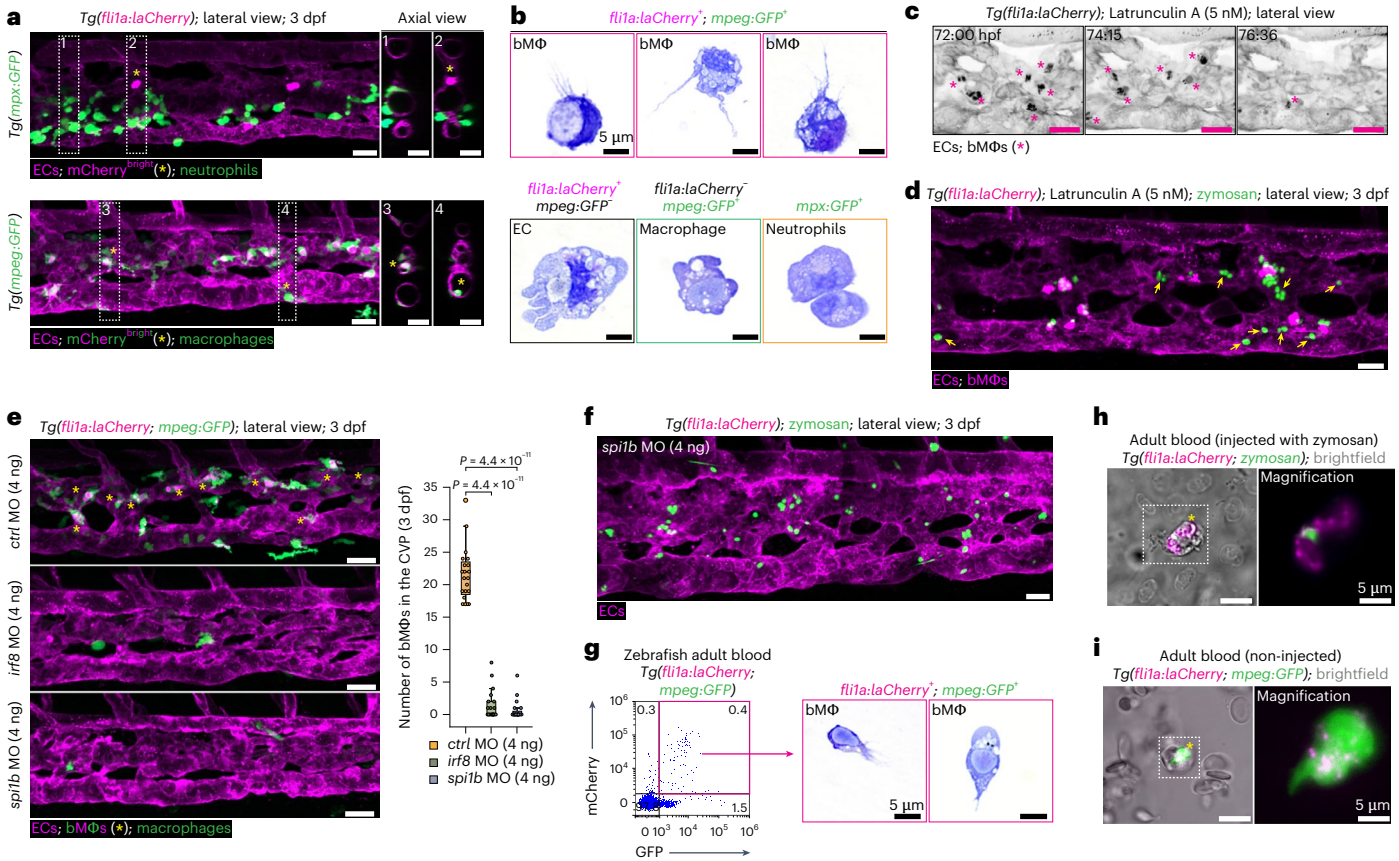

Fig. 2 | Fli1a mCherry^{bright} cells are macrophages depending on the myeloid transcription factors *spi1b* and *irf8*. **a**, Images of the CVP of 3-dpf *Tg(fli1a:laCherry; mpx:GFP)* (top) and *Tg(fli1a:laCherry; mpeg:GFP)* (bottom) embryos, where neutrophils and macrophages are marked by GFP (green), respectively. All ECs are marked by mCherry (magenta). Asterisks depict mCherry^{bright} cells. **b**, Images of bMΦs, ECs, tissue macrophage and neutrophils sorted by flow cytometry based on the indicated fluorophores after May–Grünwald Giemsa staining. **c**, Still images of Supplementary Video 5 in which a 3-dpf *Tg(fli1a:laCherry)* embryo was treated with Latrunculin A. Asterisks indicate bMΦs. **d**, Image of the CVP of a 3-dpf *Tg(fli1a:laCherry)* embryo pretreated for 1 h with Latrunculin A, followed by an intravascular injection of zymosan particles (green). Arrows indicate nonphagocytosed zymosan. **e**, Images and quantification of bMΦs in the CVP of 3-dpf *Tg(fli1a:laCherry; mpeg:GFP)* embryos injected with a control, *irf8* or *spi1b* MO (4 ng). **f**, Still image of Supplementary Video 6 in which zymosan particles were intravascularly injected in a 3-dpf *spi1b* morphant (*Tg(fli1a:laCherry)*). **g**, Representative flow cytometry plot and gating strategy for sorting bMΦs from adult *Tg(fli1a:laCherry; mpeg:GFP)* zebrafish blood. Sorted cells were cytocentrifuged (cytospin) and stained by May–Grünwald Giemsa before imaging. Representative pictures of bMΦs. **h**, Representative images of a blood smear of adult *Tg(fli1a:laCherry; mpeg:GFP)* zebrafish. **i**, Representative images of a blood smear of adult *Tg(fli1a:laCherry)* zebrafish retro-orbitally injected with zymosan. Images are representative of $n = 3$ independent experiments (30 embryos analyzed in total) (**a**), $n = 4$ independent sorts and cytospins (**b**), $n = 2$ independent time-lapse experiments (**c**, **d** and **f**) and $n = 2$ (20 embryos) (**e**). The flow cytometry plot is a representative of $n = 3$ (4 adults/n) independent experiments (**g**), and images are representative of $n = 2$ (4 adults/n) independent experiments (**h** and **i**). Percentages of populations are indicated in the quadrants and gates of each plot. Scale bars, 20 µm (**a** and **c**–**f**) and 5 µm (**b**). The box plot shows the median (center), first and third quartiles (bounds) and 1.5 times the interquartile range (whiskers) (**e**). Statistical analysis was performed using a Kruskal–Wallis test followed by Dunn's multiple comparisons test versus WT (**e**).

Extended Data Fig. 4a,b and Supplementary Video 14). Consistently, venous ECs photoconverted in the PCV at 24 hpf could be traced into the caudal vein (CV) 1 day later (Extended Data Fig. 4c). While the DA and PCV stopped producing bMΦs after ~30 hpf, venous ECs in the CVP continued producing bMΦs up to 3 dpf (Fig. 4b,c, Extended Data Fig. 4d and Supplementary Videos 15 and 16). bMΦ production involved rapid morphological changes in ECs, enabling them to emerge directly as bMΦs from the vessel wall into the circulation, with mCherry adopting its characteristic appearance. We termed this process endothelial-to-macrophage transition (EMacT). Thus, bMΦ production starts just after the initiation of circulation (~25 hpf) from both arterial and venous ECs of the DA and PCV and becomes restricted to the CVP around 30 hpf.

To further explore the capacity of the CVP to produce bMΦs, we prevented their production by injecting a low dose of *spi1b* MO (2 ng), which interfered with *spi1b* mRNA splicing up to 3 dpf (Extended Data Fig. 4e). In these embryos, the CVP started to produce bMΦs de novo from 3 dpf onward (Fig. 4d,e and Extended Data Fig. 4f). A higher *spi1b* MO dose (4 ng) caused an additional 1-day delay in bMΦ production (Fig. 4e). These de novo produced bMΦs were functional, phagocytosing intravascularly injected zymosan (Extended Data Fig. 4g). Mosaic overexpression of *spi1b* in ECs increased the number of ECs undergoing EMacT, and consequently the number of bMΦs, but this occurred at the expense of vascular morphology and integrity. (Fig. 4f, asterisk, and Extended Data Fig. 4h, magenta arrow). Importantly, some venous *spi1b*-expressing ECs (mClover^{+}) did not undergo EMacT (Fig. 4f, yellow arrows, and Extended Data Fig. 4h, yellow arrows), suggesting that not all ECs are competent for this transition.

Arterial ECs in the floor of the DA (in the aorta–gonad–mesonephros (AGM) region) produce HSPCs via a *Runx1*-dependent endothelial-to-hematopoietic transition[28–32]. In *runx1* morphants, the number of bMΦs remained normal, while the number of HSPCs was significantly reduced (Fig. 4g and Extended Data Fig. 4i). Furthermore, bMΦs lacked co-expression of the HSPC markers *cd41* or *gata2b*

(Extended Data Fig. 4j), confirming that bMΦs do not originate from HSPCs but instead arise through a novel *runx1*-independent EMacT that persists in the CVP until at least 5 dpf.

To gain further insight into the cellular and molecular difference between bMΦs, ECs and tissue macrophages, we sorted ~5,000 cells of each population and performed mass spectrometry (Extended Data Fig. 5a). We identified 55 unique proteins in bMΦs, 95 shared with tissue macrophages and 33 shared with ECs (Fig. 5a,b and Extended Data Fig. 5b). Filtering for proteins with known function in myelopoiesis, endothelial biology and adhesion (Fig. 5c) revealed a notable lack of detection of colony-stimulating factor 1 receptor (Csf1r or M-csfr) in bMΦs (Fig. 5c). Animals deficient in Csf1r are largely macrophage deficient[33,34]. To test whether the lack of csf1r affected bMΦ production and/or function, we intercrossed *csfr1a*$^{+/-}$*csfr1b*$^{+/-}$ zebrafish[35] and found a reduction in tissue macrophage numbers but normal numbers and distribution of bMΦs in double mutants (*csf1ra*$^{-/-}$*b*$^{-/-}$) (Fig. 5d,e). These bMΦs were functional, phagocytosing intravascularly injected zymosan (Extended Data Fig. 5c) and responding to endothelial damage (Extended Data Fig. 5d and Supplementary Video 17). HSPC numbers colonizing the CHT in *csf1r* double mutants at 3 dpf were unchanged (Extended Data Fig. 5e), suggesting that bMΦs alone are sufficient for normal HSPC production in the AGM and expansion in the CHT. However, in the *irf8* and *spi1b* morphants, where all macrophages are absent, HSPC numbers were similarly unaffected (Extended Data Fig. 5f). This probably reflects an accumulation of stressed HSPCs, which would typically be eliminated, coupled with a decrease in proliferating HSPCs[36], both processes probably regulated by bMΦs, ultimately resulting in no net change in HSPC numbers at 2 and 3 dpf.

In addition, we performed single-cell RNA sequencing (scRNA-seq) on bMΦs, tissue macrophages and neutrophils sorted from wild-type (WT) zebrafish, and on bMΦs and metaphocytes from *csf1ra*$^{-/-}$*b*$^{-/-}$ mutants[35]. bMΦs and tissue macrophages clustered together (in clusters 0, 3 and 4), separately from neutrophils (clusters 1 and 5) and metaphocytes (cluster 2), supporting the notion that bMΦs are molecularly distinct from these lineages (Fig. 5f,g and Extended Data Fig. 6a,b). Clusters 0 and 3 were enriched for classical macrophage markers such as *marco*, *coro1a*, *mpeg1.1*, *spi1b* and/or *mfap4* (Fig. 5h). Most bMΦs (80% from both WT and *csf1ra*$^{-/-}$*b*$^{-/-}$ mutants) resided in cluster 0, which also included a small fraction (17%) of tissue macrophages (Fig. 5g). Consistently, bMΦs sorted from zymosan injected embryos (bMΦs zymosan^{+}; cluster 10) clustered adjacent to cluster 0 and additionally expressed inflammatory/activation-associated genes (*tnfa*, *il1b* and *dram1)* (Extended Data Fig. 6c,d). Thus, cluster 0 is enriched for functional bMΦs, which exhibit high expression of macrophage markers as well as some endothelial markers (*fli1b*, *mrc1b*, *lamp2*, *cxcl8a* and *itgav*) (Fig. 5h). Because cluster 4 was characterized by the expression of *dnmt3bb1*, *myb* and *gata2b*[37–39] —representing HSPCs/myeloid progenitors that are also marked by the *fli1a:laCherry;mpeg:GFP* transgenes (Fig. 5h)—we excluded cluster 4 from further analysis and show that bMΦs do express endothelial and macrophage markers (Fig. 5i). Aside from slightly lower expression of some pro-inflammatory markers (Fig. 5j,k), bMΦs from WT and *csf1ra*$^{-/-}$*b*$^{-/-}$ mutants were transcriptionally nearly identical. This reinforces that bMΦs are generated and function independently of *csf1ra* and *csf1rb*, despite low-level transcript expression in some bMΦs (Extended Data Fig. 6e). Together, these data support our functional and imaging data that bMΦs represent a distinct subset of bona fide macrophages, characterized by the co-expression of macrophage and endothelial markers. Although molecularly similar to tissue macrophages, bMΦs are distinguished by their morphology, function and intravascular localization.

Using a similar approach as in zebrafish, we analyzed blood from adult and neonate mice 1 h after intravenous zymosan injection by multicolor flow cytometry. Zymosan particles were phagocytosed by cells with the following phenotype: CSF1R$^{-/(low)}$ CX3CR1^{-} CD11b^{+} Ly6C^{high} Ly6G^{-} CD43^{+} CD31^{+} F4/80^{-} (Extended Data Fig. 7a,b (adult blood); Extended Data Fig. 7c,d (neonatal blood); Extended Data Fig. 8a,b (controls)). This signature differs from known circulating myeloid populations, including patrolling/nonclassical monocytes (NCMs) (CSF1R^{+} CX3CR1^{high} CD11b^{+} Ly6C$^{Low/-}$ CD43^{+} CD31^{-})[11,40] (Extended Data Fig. 8c,d), classical monocytes (CSF1R^{+} CX3CR1^{low} CD11b^{+} Ly6C^{high} CD43^{low}) and neutrophils (Ly6G^{+}). NCMs were nearly depleted from the blood following zymosan injection (Extended Data Fig. 8e), whereas bMΦs remained in circulation (Extended Data Fig. 7a–d). In addition to sharing phagocytic capacity and phenotypic features (CSF1R^{-} CD31^{+} (endothelial marker)) with zebrafish bMΦs, their mouse counterparts also displayed a similar morphology with pseudopod-like extensions (Extended Data Figs. 7d and 8f), strongly suggesting that bMΦs are evolutionarily conserved.

Here, we identify a specialized and conserved population of macrophages that reside and function within the vasculature of zebrafish and mice, termed bMΦs. These cells maintain blood homeostasis by catching, assessing and either releasing or phagocytosing circulating foreign particles and abnormal endogenous cells, a process recently dubbed 'grooming' and 'dooming'[36]. bMΦs also act as primary responders to endothelial damage, clearing endothelial debris, whereas tissue macrophages and neutrophils contribute minimally. Whether bMΦs are required for blood vessel maintenance and function, analogous to perivascular macrophages in skin capillaries[41] or microglia in the brain[42,43], remains unknown and will require tissue-specific or conditional knockout strategies.

bMΦs persist beyond development into adulthood with similar phenotype and function. Whether these adult bMΦs have an embryonic origin and are maintained locally through self-renewal, or are produced de novo through EmacT, remains unresolved. Notably, bMΦ formation and function are preserved in *csf1r*-deficient embryos that lack nearly all other tissue macrophages[35,44–46]. Because Csf1r is broadly expressed across tissue macrophages, the *Csf1r-EGFP* mouse line (MacGreen) is widely used to detect and visualize macrophages[47]. The lack of Csf1r detection in bMΦs probably explains why they have remained unnoticed thus far.

Macrophages in zebrafish have three established origins: the rostral blood island (primitive macrophages), the posterior blood island (via

Fig. 3 | bMΦs maintain blood homeostasis and respond to vascular damage. **a**,**b**, Still images of Supplementary Videos 7 (**a**) and 8 (**b**), illustrating the catching, assessment and release (**a**) or phagocytosis (**b**) of erythrocytes by bMΦs, respectively, in the CVP of *Tg(fli1a:laCherry;globin:GFP)* embryos in which erythrocytes are GFP^{+} (*globin*, arrow) and bMΦs are mCherry^{bright} (*fli1a*, asterisk). Arrows in the magnification image show the intimate contact between the erythrocyte and bMΦ. **c**, Still images of Supplementary Video 10, showing the interactions between HSPCs that are marked by GFP (*gata2b*, arrows) and bMΦs that are mCherry^{bright} (*fli1a*, asterisk). **d**, Images of the CVP region of a 3-dpf *Tg(fli1a:laCherry;cd41:GFP)* embryo, where HSPCs are GFP^{+} (*cd41*) and bMΦs are mCherry^{bright} (*fli1a*). The asterisk indicates a bMΦ that engulfed cytoplasmic material of a GFP^{+} HSPC. The dashed square is shown enlarged in the right image. **e**, Time-lapse still images illustrating the phagocytosis of a HSPC by a bMΦ. In the CVP of 3-dpf *Tg(fli1a:laCherry;gata2b:KalTA4;uas:laGFP)*, HSPCs are GFP^{+} (*gata2b*, arrow) and bMΦs are mCherry^{bright} (*fli1a*, asterisk). **f**, Top: schematic representation of the optogenetic tool PhoCl2c-Bid. Upon a short UV light pulse of 405 nm, Bid is photocleaved and activated, which ultimately leads to the release of cytochrome c from the mitochondria and apoptosis of the cell. Bottom: still images of Supplementary Video 11, showing the optogenetic ablation of targeted ECs (translucent circle) in *Tg(fli1a:laCherry;fli1a:PhoCl2c-Bid-mClover;mpeg:GFP)* embryos in which tissue macrophages are GFP^{+}laCherry^{-} (arrow), ECs are GFP^{-}laCherry^{+} and bMΦs are GFP^{+}laCherry^{+} (asterisk). Images are representative of $n = 3$ independent time-lapse experiments (**a**–**f**). Scale bars, 20 µm, except for **a** (5 µm).

https://doi.org/10.1038/s41590-026-02481-y

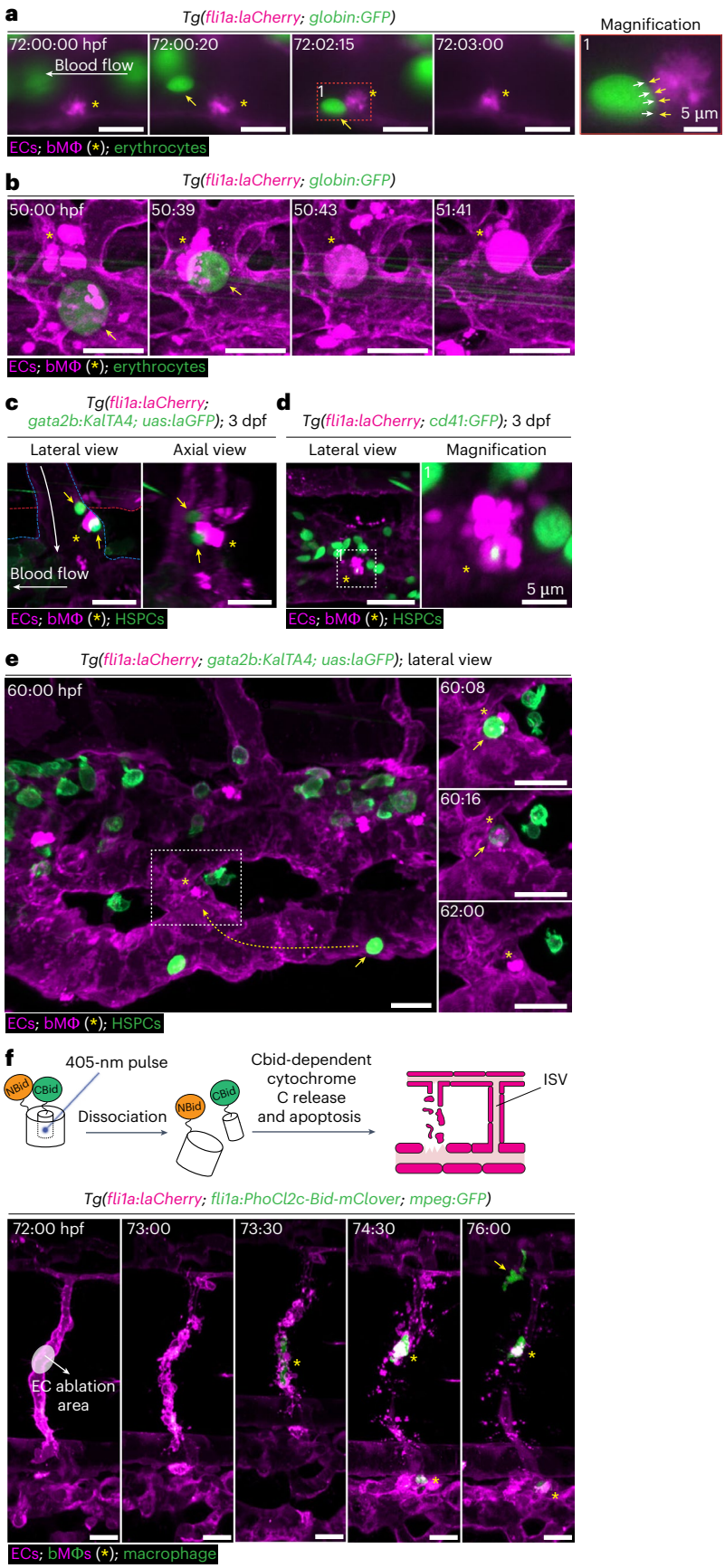

https://doi.org/10.1038/s41590-026-02481-y

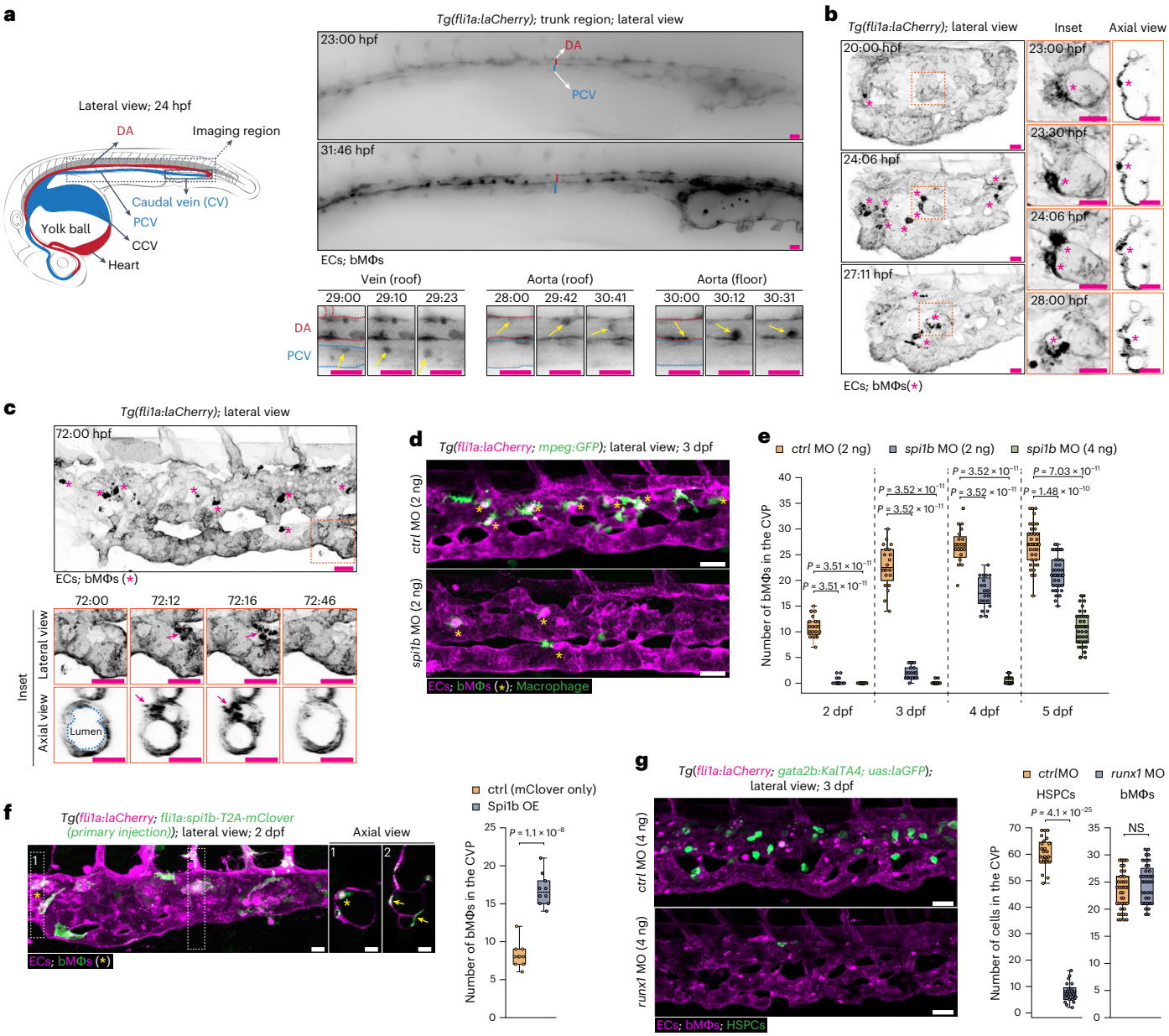

Fig. 4 | bMΦs originate from ECs that undergo a *runx1*-independent EMacT. **a**, Left: schematic representation of a 24-hpf zebrafish embryo. The dashed line indicates the imaging region (trunk). Right: still images of Supplementary Video 14 at two time points. All ECs are marked by laCherry (black). Bottom: insets from different locations and time to illustrate the emergence of bMΦs (arrows). **b**, Still images of Supplementary Video 15. CVP region of a *Tg(fli1a:laCherry)* embryo. Orange boxes represent the insets shown on the left. Asterisks show venous ECs undergoing EMacT toward the luminal of the CV. **c**, Time-lapse still images, showing the transition of a venous EC into a bMΦ through EMacT (arrows). Asterisks: bMΦs already present in the CVP. Insets are a magnification of the dashed orange box in the top panel, shown in lateral and axial views. **d**,**e**, Images (**d**) and quantification (**e**) of bMΦs in the CVP of *Tg(fli1a:laCherry; mpeg:GFP)* embryos after *control* (*ctrl*) MO, or low (2 ng) or high (4 ng) doses of *spi1b* MO injection. Asterisks indicate de novo generated bMΦs (mCherry^{bright}GFP^{+}). **f**, Images and quantification of bMΦs in the CVP of 2-dpf *Tg(fli1a:laCherry; fli1a:spi1b-T2A-mClover)* embryos, showing ectopically produced bMΦs by mosaic OE of *Spi1b-T2A-laClover*. The asterisk depicts a bMΦ. Arrows depict ECs expressing *Spi1b* that did not undergo EMacT. **g**, Images and quantification of HSPCs and bMΦs in the CVP of *Tg(fli1a:laCherry; gata2b:KalTA4; uas:laGFP)* embryos after *ctrl* MO and *runx1* MO injection. HSPCs are GFP^{+} (*gata2b*), and bMΦs are mCherry^{bright} (*fli1a*). Images are representative of $n = 3$ independent time-lapse experiments (**a**–**c**), $n = 2$ (2, 3 and 4 dpf, 20 embryos per condition; 5 dpf, 41 embryos per condition) (**d** and **e**), $n = 2$ (10 embryos) (**f**), $n = 2$ (*ctrl* MO HSPCs, 24 embryos; bMΦs, 42 embryos; *runx1* MO HSPCs, 24 embryos; bMΦs, 40 embryos) (**g**). Scale bars, 20 µm. OE, overexpression; NS, not significant. Box plots show the median (center), first and third quartiles (bounds) and 1.5 times the interquartile range (whiskers) (**e**–**g**). Statistical analysis was performed using a Kruskal–Wallis test followed by Dunn's multiple comparisons test versus WT (**e**) and a two-tailed Mann–Whitney *U* test for comparison of two conditions (**f** and **g**).

EMPs) and the ventral endothelial wall of the DA (via HSPCs). We now introduce a fourth origin generating intravascular bMΦs dedicated to blood and vessel homeostasis. bMΦs arise directly through an unexpected EMacT, depending on *irf8* and *spi1b* but not *runx1*. Ectopic *spi1b* expression forces some venous ECs to undergo EMacT, while others do not, supporting the heterogeneity of PCV and caudal vein ECs, which can adopt arterial, venous, lymphatic[48] or, as shown here, myeloid fates.

We also identified bMΦ-like cells in neonatal and adult mouse blood, which are phenotypically distinct from circulating myeloid populations (patrolling monocytes/NCMs, classical monocytes

https://doi.org/10.1038/s41590-026-02481-y

and neutrophils). bMΦs also differ from macrophages derived from CX3CR1^{+}CSF1R^{+} endothelial–macrophage progenitors, which do not circulate and are confined to the aortic adventitia[49]. Murine bMΦ-like cells exhibit phagocytic capacity and share phenotypic and morphological similarities with zebrafish bMΦs, suggesting that they represent true and evolutionarily conserved bMΦs. These findings challenge current views of blood and vascular system maintenance and might pave the way for using bMΦs or bioengineered versions to target blood-related diseases, as well as cardiovascular diseases involving endothelial damage.

Fig. 5 | *Csf1r*-independent production of bMΦs. a, Venn diagram showing shared and distinct proteins per cell population. **b**, Three-dimensional plot of clustered proteins by *K*-means clustering. **c**, Heatmap of proteins involved in myeloid differentiation, EC biology or cell adhesion. **d**, Image of the CVP of 3-dpf *Tg(fli1a:laCherry;mpeg:GFP) csf1ra*$^{-/-}$*b*$^{-/-}$ (double mutant). Asterisks depict bMΦs. **e**, Top: quantification of tissue macrophages (Macs) in the trunk region of the indicated offspring of an incross of *Tg(fli1a:laCherry;mpeg:GFP) csf1ra*$^{+/-}$*csf1rb*$^{+/-}$ (referred to as *csf1ra*$^{+/-}$*b*$^{+/-}$) zebrafish. Bottom: quantification of bMΦs in the CVP of the offspring of an incross of *Tg(fli1a:laCherry;mpeg:GFP) csf1ra*$^{+/-}$*b*$^{+/-}$ zebrafish. **f**, UMAP scatter plot after unsupervised clustering of scRNA-seq data. **g**, Distribution of the sorted cell types in the different clusters shown in **f**. **h**, Dot plot representing the average expression and percent of cells expressing a selection of HSPC, macrophage and endothelial genes, expressed in the different clusters shown in **f**. **i**, Violin plots of gene expression levels of *mpeg1.1*, *marco*, *mfap4*, *mfapbb*, *fli1b*, *lamp2* and *itgav*, comparing bMΦs (WT), bMΦs (*csf1ra*$^{-/-}$*b*$^{-/-}$), tissue macrophages, metaphocytes and neutrophils. **j**, Hallmark pathway enrichment in bMΦs from WT or *csf1ra*$^{-/-}$*b*$^{-/-}$ embryos. **k**, Violin plots of gene expression levels of *il1b*, *tnfb*, *dram1*, *c1qa* and *cfp*, comparing bMΦs from WT and *csf1ra*$^{-/-}$*b*$^{-/-}$ embryos. Images are representative of $n = 5$ independent experiments (5 embryos) (**d**), and quantification is from $n = 1$ experiment (138 embryos) (**e**). Box plots show the median (center), first and third quartiles (bounds) and 1.5 times the interquartile range (whiskers) (**e**). Statistical analysis was performed using a Kruskal–Wallis test followed by Dunn's multiple comparisons test versus WT (**e**). log IBAQ, log Intensity-Based Absolute Quantification.

Online content

Any methods, additional references, Nature Portfolio reporting summaries, source data, extended data, supplementary information, acknowledgements, peer review information; details of author contributions and competing interests; and statements of data and code availability are available at https://doi.org/10.1038/s41590-026-02481-y.

References

1. Gordon, S. & Plüddemann, A. Tissue macrophages: heterogeneity and functions. *BMC Biol.* **15**, 53 (2017).
2. Mass, E., Nimmerjahn, F., Kierdorf, K. & Schlitzer, A. Tissue-specific macrophages: how they develop and choreograph tissue biology. *Nat. Rev. Immunol.* **23**, 563–579 (2023).
3. Wynn, T. A., Chawla, A. & Pollard, J. W. Macrophage biology in development, homeostasis and disease. *Nature* **496**, 445–455 (2013).
4. Hashimoto, D. et al. Tissue-resident macrophages self-maintain locally throughout adult life with minimal contribution from circulating monocytes. *Immunity* **38**, 792–804 (2013).
5. Gomez Perdiguero, E. et al. Tissue-resident macrophages originate from yolk-sac-derived erythro-myeloid progenitors. *Nature* **518**, 547–551 (2015).
6. Hoeffel, G. et al. C-Myb(+) erythro-myeloid progenitor-derived fetal monocytes give rise to adult tissue-resident macrophages. *Immunity* **42**, 665–678 (2015).
7. Bertrand, J. Y. et al. Definitive hematopoiesis initiates through a committed erythromyeloid progenitor in the zebrafish embryo. *Development* **134**, 4147–4156 (2007).
8. Elchaninov, A., Vishnyakova, P., Menyailo, E., Sukhikh, G. & Fatkhudinov, T. An eye on Kupffer cells: development, phenotype and the macrophage niche. *Int. J. Mol. Sci.* **23**, 9868 (2022).
9. Kurotaki, D., Uede, T. & Tamura, T. Functions and development of red pulp macrophages. *Microbiol. Immunol.* **59**, 55–62 (2015).
10. An, H. et al. Splenic red pulp macrophages eliminate the liver-resistant Streptococcus pneumoniae from the blood circulation of mice. *Sci. Adv.* **11**, eadq6399 (2025).
11. Auffray, C. et al. Monitoring of blood vessels and tissues by a population of monocytes with patrolling behavior. *Science* **317**, 666–670 (2007).
12. Lawson, N. D. & Weinstein, B. M. In vivo imaging of embryonic vascular development using transgenic zebrafish. *Dev. Biol.* **248**, 307–318 (2002).
13. Renshaw, S. A. et al. A transgenic zebrafish model of neutrophilic inflammation. *Blood* **108**, 3976–3978 (2006).
14. Ellett, F., Pase, L., Hayman, J. W., Andrianopoulos, A. & Lieschke, G. J. mpeg1 promoter transgenes direct macrophage-lineage expression in zebrafish. *Blood* **117**, e49–e56 (2011).
15. Hogan, B. M. et al. Ccbe1 is required for embryonic lymphangiogenesis and venous sprouting. *Nat. Genet.* **41**, 396–398 (2009).
16. van Impel, A. et al. Divergence of zebrafish and mouse lymphatic cell fate specification pathways. *Development* **141**, 1228–1238 (2014).
17. Prajsnar, T. K. et al. Zebrafish as a novel vertebrate model to dissect enterococcal pathogenesis. *Infect. Immun.* **81**, 4271–4279 (2013).
18. Nourshargh, S. & Alon, R. Leukocyte migration into inflamed tissues. *Immunity* **41**, 694–707 (2014).
19. Kress, H. et al. Filopodia act as phagocytic tentacles and pull with discrete steps and a load-dependent velocity. *Proc. Natl Acad. Sci. USA* **104**, 11633–11638 (2007).
20. Lugo-Villarino, G. et al. Identification of dendritic antigen-presenting cells in the zebrafish. *Proc. Natl Acad. Sci. USA* **107**, 15850–15855 (2010).
21. El Sherbini, H. et al. Lectin ligands on human dendritic cells and identification of a peanut agglutinin positive subset in blood. *Cell. Immunol.* **200**, 36–44 (2000).
22. Rhodes, J. et al. Interplay of pu.1 and gata1 determines myelo-erythroid progenitor cell fate in zebrafish. *Dev. Cell* **8**, 97–108 (2005).
23. Rosenbauer, F. & Tenen, D. G. Transcription factors in myeloid development: balancing differentiation with transformation. *Nat. Rev. Immunol.* **7**, 105–117 (2007).
24. Tamura, T., Nagamura-Inoue, T., Shmeltzer, Z., Kuwata, T. & Ozato, K. ICSBP directs bipotential myeloid progenitor cells to differentiate into mature macrophages. *Immunity* **13**, 155–165 (2000).
25. Li, L., Jin, H., Xu, J., Shi, Y. & Wen, Z. Irf8 regulates macrophage versus neutrophil fate during zebrafish primitive myelopoiesis. *Blood* **117**, 1359–1369 (2011).
26. Lu, X. et al. Photocleavable proteins that undergo fast and efficient dissociation. *Chem. Sci.* **12**, 9658–9672 (2021).
27. Weijts, B. et al. Endothelial struts enable the generation of large lumenized blood vessels de novo. *Nat. Cell Biol.* **23**, 322–329 (2021).
28. Bertrand, J. Y. et al. Haematopoietic stem cells derive directly from aortic endothelium during development. *Nature* **464**, 108–111 (2010).
29. Kissa, K. & Herbomel, P. Blood stem cells emerge from aortic endothelium by a novel type of cell transition. *Nature* **464**, 112–115 (2010).
30. Chen, M. J., Yokomizo, T., Zeigler, B. M., Dzierzak, E. & Speck, N. A. Runx1 is required for the endothelial to haematopoietic cell transition but not thereafter. *Nature* **457**, 887–891 (2009).
31. Kalev-Zylinska, M. L. et al. Runx1 is required for zebrafish blood and vessel development and expression of a human RUNX1-CBF2T1 transgene advances a model for studies of leukemogenesis. *Development* **129**, 2015–2030 (2002).
32. Boisset, J.-C. et al. In vivo imaging of haematopoietic cells emerging from the mouse aortic endothelium. *Nature* **464**, 116–120 (2010).
33. MacDonald, K. P. A. et al. An antibody against the colony-stimulating factor 1 receptor depletes the resident subset of monocytes and tissue- and tumor-associated macrophages but does not inhibit inflammation. *Blood* **116**, 3955–3963 (2010).

34. Dai, X.-M. et al. Targeted disruption of the mouse colony-stimulating factor 1 receptor gene results in osteopetrosis, mononuclear phagocyte deficiency, increased primitive progenitor cell frequencies, and reproductive defects. *Blood* **99**, 111–120 (2002).
35. Kuil, L. E. et al. Zebrafish macrophage developmental arrest underlies depletion of microglia and reveals Csf1r-independent metaphocytes. *eLife* **9**, e53403 (2020).
36. Wattrus, S. J. et al. Quality assurance of hematopoietic stem cells by macrophages determines stem cell clonality. *Science* **377**, 1413–1419 (2022).
37. Butko, E. et al. Gata2b is a restricted early regulator of hemogenic endothelium in the zebrafish embryo. *Development* **142**, 1050–1061 (2015).
38. Gore, A. V. et al. Epigenetic regulation of hematopoiesis by DNA methylation. *eLife* **5**, e11813 (2016).
39. Thompson, M. A. et al. The cloche and spadetail genes differentially affect hematopoiesis and vasculogenesis. *Dev. Biol.* **197**, 248–269 (1998).
40. Carlin, L. M. et al. Nr4a1-dependent Ly6C(low) monocytes monitor endothelial cells and orchestrate their disposal. *Cell* **153**, 362–375 (2013).
41. Mesa, K. R. et al. Niche-specific dermal macrophage loss promotes skin capillary ageing. *Nature* **648**, 173–181 (2025).
42. Bisht, K. et al. Capillary-associated microglia regulate vascular structure and function through PANX1–P2RY12 coupling in mice. *Nat. Commun.* **12**, 5289 (2021).
43. Haruwaka, K. et al. Dual microglia effects on blood brain barrier permeability induced by systemic inflammation. *Nat. Commun.* **10**, 5816 (2019).
44. Rojo, R. et al. Deletion of a Csf1r enhancer selectively impacts CSF1R expression and development of tissue macrophage populations. *Nat. Commun.* **10**, 3215 (2019).
45. Oosterhof, N. et al. Colony-stimulating factor 1 receptor (CSF1R) regulates microglia density and distribution, but not microglia differentiation in vivo. *Cell Rep.* **24**, 1203–1217 (2018).
46. Hason, M. et al. M-CSFR/CSF1R signaling regulates myeloid fates in zebrafish via distinct action of its receptors and ligands. *Blood Adv.* **6**, 1474–1488 (2022).
47. Sasmono, R. T. et al. A macrophage colony-stimulating factor receptor-green fluorescent protein transgene is expressed throughout the mononuclear phagocyte system of the mouse. *Blood* **101**, 1155–1163 (2003).
48. Nicenboim, J. et al. Lymphatic vessels arise from specialized angioblasts within a venous niche. *Nature* **522**, 56–61 (2015).
49. Williamson, A. E. et al. Discovery of an embryonically derived bipotent population of endothelial-macrophage progenitor cells in postnatal aorta. *Nat. Commun.* **15**, 7097 (2024).

Methods

Animals

All animal procedures performed at the Hubrecht Institute were approved by the local animal experiment committee and by the Animal Experimentation Committee (DEC) of the Royal Netherlands Academy of Arts and Sciences. Experiments were performed according to the national and European animal welfare laws, guidelines and policies.

Zebrafish husbandry

The following zebrafish lines were previously described: *Tg(fli1a:lifeactCherry)*^{ncv7Tg} (ref. 50) referred to as *fli1a:laCherry*; *Tg(hbbe1.1:EGFP)*^{zf446} (ref. 51) referred to as *Tg(globin:eGFP); Tg(UAS:lifeactGFP)*^{mu271} (ref. 52) referred to as *UAS:laGFP*; *Tg(gata2b:KalTA4)*[37]; *Tg(-6.0itga2b:eGFP)*^{la2} (ref. 53) referred to as *cd41:eGFP*; *Tg(mpeg:eGFP)*^{gl22} (ref. 14); *Tg(mpx:eGFP)*[13]; *Tg(kdrl:Hsa.HRAS-mCherry)*[15] referred to as *kdrl:mCherry-CAAX*; *csf1ra*^{j4e1} (ref. 54); *csf1rb*^{re01} (ref. 55); *Tg(Ola.flt4:Gal4FF)*^{hu9236Tg} (ref. 16), *Tg(flk1:Dendra2)*[56] referred to as *kdrl:Dendra*, *Tg(mpeg:Gal4.VP-16)*^{sh256} (ref. 17) referred to as *mpeg:Gal4*, *Tg(UAS-E1B:NTR-mCherry)*[57] referred to as *UAS:mCherry*, *Tg(kdrl:GFP)*[58].

Morpholino, plasmid injection and chemical treatment

Embryos were injected at the one-cell stage with MOs (GeneTools) or 50 ng plasmid with 100 ng tol2 mRNA. *Spi1b* (*pu.1*) translation blocking MO (5′-GATATACTGATACTCCATTGGTGGT-3′)[22]; *irf8* splice-site MO (5′- AATGTTTCGCTTACTTTGAAAATGG-3′)[25]; *runx1* splice-site MO, (5′- AGCGCTCTTACCGTATTTGGCGTCC-3′)[59]; and scrambled MO (control) were injected at similar concentrations to the targeted MO (5′-CCTCTTACCTCAGTTACAATTTATA-3′). Capped tol2 mRNA was synthesized from linearized pCS2+ constructs using the mMessage mMachine SP6 kit (Ambion, AM1340). Embryos were treated with 5 nM Latrunculin A (Cayman Chemical, #10010630) dissolved in ethanol (stock 2,000×). Control embryos were treated with ethanol alone (2,000× diluted).

Intravascular and intratissue injections of particles or cells

Zebrafish embryos were injected with Zymosan A (*Saccharomyces cerevisiae*) BioParticles conjugated with Alexa Fluor 488 (Invitrogen), COMPEL magnetic COOH-modified beads (Glacial Blue; 3 µm; Bangs Labs), and *Escherichia coli* labeled with CellTracker Green CMFDA (Invitrogen), prepared according to the manufacturer's instructions. Blood from adult *Tg(globin:GFP)* fish was collected from the DA using a glass microcapillary needle coated with heparin (5 mg ml^{-1} dissolved in saline), as previously described[60]. Particles and cells were injected into the CCV (Fig. 1a) or into the tissue adjacent to the CVP.

For adult zebrafish, zymosan injection was done retro-orbitally as previously described[61].

In adult mice, zymosan (2×10^6 particles) was injected into the tail vein of adult C57BL/6 mice, and blood was collected retro-orbitally 1 h post-injection.

In neonatal mice, single C57BL/6 neonates (P2) were placed directly on wet ice for 30–60 s to anesthetize the animal. Then, 50 µl of zymosan (3.33×10^5 particles) was injected into the temporal (or facial) vein, located just anterior to the ear bud on one side of the head, using a dissecting microscope. After injection, the neonates recovered and rewarmed within 2–3 min and were placed back into the cage with a heating pad underneath to facilitate recovery (as described in ref. 62). Blood was collected 1 h post-injection by decapitation. Blood was collected using a heparinized glass capillary into an EDTA-coated Eppendorf tube. All tubes were stored on ice for later flow cytometry analysis or sorting.

Morpholino check

To validate the *spi1b* MO, we isolated total RNA from the indicated time point with the RNeasy mini kit (Qiagen) following the manufacturer's instructions, including the DNAse treatment. cDNA was synthesized with Superscript III (Thermo Fisher) by using a random hexamer primer. A normal polymerase chain reaction (PCR) was run with the forward primer (5′-AGAGAGGGTAACCTGGACTGG-3′) on exon 2 and the reverse primer (5′-CCACTGGATGAATGTGATGC-3′) on exon 4. PCR product was run on a 2% agarose gel, giving a product of 200 bp in WT embryos.

Cloning and generation of transgenic lines

To generate the *Tg(fli1a:spi1b-T2A-laClover)* construct, we cloned the coding sequence of zebrafish *Spi1b* (ENSDARG00000000767) in frame with the T2A sequence (5′-GAGGGCAGAGGCAGTCTGCTGACATGCG-GTGACGTGGAAGAGAATCCCGGCCCT-3′) and lifeact-mClover3 at its C terminal. PCR products were ligated in front of the partial *fli1a* promoter[50], flanked by Tol2 sites, using the Gibson Cloning method (NEB HiFi DNA Assembly Mix, E2621S). The optogenetic apoptosis construct was generated by subcloning the NBid-PhoCl2c-CBid[26] (Addgene plasmid #164051) and placing it with a T2A sequence and mClover3 in front of the *fli1a* promoter that was flanked with Tol2 sites. To generate *Tg(UAS:laCherry)*, we cloned the lifeact tag N-terminally 5′-ATGGGTGTCGCAGATTTGATCAAGAAATTCGAAAGCATCTCAAA-GGAAGAA-3′) of mCherry and cloned it into a 4× nonrepetitive UAS[63] plasmid containing Tol2 sites.

Genotyping

For the genotyping of the *csf1ra* locus, we used a standard PCR protocol with an annealing temperature of 58 °C and the following primers: forward (5′-CCTTTAACGCTGATGTGTGC-3′) and reverse (5′-GGAGCAAACCTTGCAGAGC-3′). On completion of the PCR run, 0.1 µl of the restriction enzyme BssSI-v2 (NEB) was directly added to the reaction and incubated >1 h at 37 °C and run on a 3% gel. A single band of 242 bp can be detected in WT animals, and two bands of 123 + 119 bp can be detected in homozygous mutants. For the *csf1rb* locus, a similar strategy was used with the primer set forward (5′- CTTGCTGACAAATCCAGCAG-3′), reverse (5′- GAGCTAACCGGACAAACTGG-3′) and MspI (NEB) restriction enzyme. WT bands after digestion are 203, 132 and 71 bp, whereas homozygous mutant bands are 331 and 71 bp.

EC ablation and photoconversion

To ablate ECs in the *Tg(fli1a:spi1b-T2A-mClover3)* embryos or to photoconvert ECs in the *Tg(kdrl:Dendra)* embryos, we drew the desired shape around the targeted ECs with experimental region tool in ZEN 3.9 software (Zeiss). This region was used to expose ECs to 100% 405-nm light for ~10 s using the interactive bleaching tool.

Microscopy and postprocessing imaging

Live microscopy was done in environmentally controlled microscopy system based on a Leica Thunder Imager or a Zeiss LSM 900 with Airyscan2. For all imaging, embryos were placed into a modified Four-Well WillCo dish[64] submerged in E3 medium containing 0.168 mg ml^{-1} = 0.0168% ≈ 0.02% ethyl 3-aminobenzoate methanesulfonate (MS222; Sigma E10521) at a temperature of 28.5 °C. Imaging was subsequently done with either 20×/0.75, 40×/1.4 or 63×/1.46 objectives.

Images captured in airyscan2 mode (Zeiss LSM900) were first processed in Zeiss ZEN (airyscan processing) and subsequently analyzed using FIJI or Imaris software. In some cases, *XY* drifts were corrected using the MultiStackReg plugin (FIJI; B. Busse, NICHD) and correction of fluorescence bleaching by histogram matching (FIJI). Contrast in all images was adjusted. Look-up tables were modified (red to magenta, or red/green to black and white for better visualization) using FIJI or Imaris. Videos and animations were created in Adobe After Effects.

Cell preparation, flow cytometry analysis/sorting, cytospin and staining

For zebrafish embryos, embryos were anesthetized in E3 medium containing 0.01% tricaine. After removal of medium, embryos were put

in TrypLE (ThermoFisher, 12563011) for 45 min at 32 °C with vigorous shaking. Cells were then washed with fluorescence-activated cell sorting (FACS) buffer (phosphate-buffered saline (PBS) + 2% fetal bovine serum (FBS) + 2 mM EDTA), resuspended in FACS buffer supplemented with 4′,6-diamidino-2-phenylindole (DAPI; ThermoFisher, 0.5 µg ml^{-1} final concentration) and subsequently filtered through 40-µm nylon mesh. Cells were sorted on a FACS Aria II (BD Biosciences) and collected in FACS buffer for cytospin (Thermo Shandon Cytospin 4) or in ice-cold PBS for mass spectrometry. After cytospin, slides were air-dried at room temperature and subsequently submerged in May–Grünwald solution for 10 min, rinsed in phosphate buffer and incubated in Giemsa solution for 20 min. Slides were rinsed with demi-water and air-dried at room temperature. A coverslip was mounted with Eukitt Quick-Hardening Mounting Medium (Sigma-Aldrich), and stained cells were imaged.

For zebrafish adults, blood from adult *Tg(fli1a:laCherry)* fish was collected from the DA using a glass microcapillary needle coated with heparin (5 mg ml^{-1} dissolved in saline), as previously described[60]. Blood was transferred into an EDTA-coated (1.6 mg EDTA ml^{-1}) Eppendorf tube (K3E; Sarstedt). Erythrocytes were lysed by adding 2 ml of 1× IOTest 3 Lysing Solution (Beckman Coulter) and incubated for 10 min at room temperature. Cells were washed twice with FACS buffer (PBS + 2% FBS + 2 mM EDTA), strained through a 40-µm mesh cell strainers (VWR) and resuspended in FACS buffer + DAPI (ThermoFisher, 0.5 µg ml^{-1} final concentration). Samples were acquired on a CytoFLEX cytometer (Beckman Coulter) and reanalyzed using FlowJo (BD Biosciences).

For adult and neonatal mice, blood was collected in EDTA-coated (1.6 mg EDTA ml^{-1}) Eppendorf tube (K3E; Sarstedt). Blood was diluted with FACS buffer (PBS + 2% FBS + 2 mM EDTA) to the desired concentration, and antibodies were directly added for 30 min at 4 °C. Directly after staining, the erythrocytes were lysed by adding 2 ml of 1× IOTest 3 Lysing Solution (Beckman Coulter) and incubated for 10 min at room temperature. Cells were washed twice with FACS buffer (PBS + 2% FBS + 2 mM EDTA), strained through a 40-µm mesh cell strainers (VWR) and resuspended in FACS buffer + DAPI (ThermoFisher, 0.5 µg ml^{-1} final concentration). The following antibodies were used: BD Pharmingen: CD31-PE (cat. no. 553373); CD43-APC (cat. no. 560663); CX3CR1-PE (cat. no. 567530); Ly6C-FITC (cat. no. 553104); Ly6C-APC (cat. no. 560595); Ly6G-PE (cat. no. 561104); CD115-PE (CSF1R; cat. no. 565249); CD62L-FITC (cat. no. 553150); CD11b-FITC (cat. no. 553310); CD11b-PE (cat. no. 553311); BioLegend: CX3CR1-APC (cat. no. 149007); Bio-Rad: F4/80-RPE (cat. no. MCA497G). Isotype-matched control antibodies were used for controls. Samples were acquired on a CytoFLEX cytometer (Beckman Coulter) and reanalyzed using FlowJo (BD Biosciences).

Proteomics, scRNA-seq and data analysis

Proteomics. For global proteome analysis of whole-cell extracts, cells were lysed in 100 mM Tris–HCl, pH 8.2, containing 1% sodium deoxycholate using sonication in a Bioruptor Pico (Diagenode). Protein concentrations were measured using a bicinchoninic acid assay (Thermo Fisher Scientific). For this, 100 µg protein was reduced in lysis buffer with 5 mM dithiothreitol and alkylated with 10 mM iodoacetamide. Next, proteins were digested with 2.5 µg trypsin (1:40 enzyme:substrate ratio) overnight at 37 °C. After digestion, peptides were acidified with trifluoroacetic acid to a final concentration of 0.5% and centrifuged at 10,000*g* for 10 min to spin down the precipitated sodium deoxycholate. Peptides dissolved in the supernatant were desalted on a 50-mg C18 Sep-Pak Vac cartridge (Waters). After washing the cartridge with 0.1% trifluoroacetic acid, peptides were eluted with 50% acetonitrile and dried in a Speedvac centrifuge. Peptides were then analyzed by nanoflow liquid chromatography–tandem mass spectrometry (MS/MS) as described below.

Nanoflow liquid chromatography–MS/MS was performed on an EASY-nLC system (Thermo) coupled to an Orbitrap Eclipse Tribrid mass spectrometer (both Thermo Fisher Scientific) operating in positive mode and equipped with a nanospray source. Peptide mixtures were trapped on a ReproSil C18 reversed phase column (Dr Maisch GmbH; column dimensions 1.5 cm × 100 µm, packed in-house) at a flow rate of 8 µl min^{-1}. Peptide separation was performed on ReproSil C18 reversed phase column (Dr Maisch GmbH; column dimensions 15 cm × 50 µm, packed in-house) using a linear gradient from 0% to 80% B (A = 0.1% formic acid; B = 80% (v/v) AcN, 0.1% formic acid) in 120 min and at a constant flow rate of 250 nl min^{-1}. The column eluent was directly sprayed into the electrospray Ionization source of the mass spectrometer.

All mass spectra were acquired in profile mode; the resolution in MS1 mode was set to 120,000 (automatic gain control (AGC) target: 4E5) and the *m*/*z* range to 350–1,400. Fragmentation of precursors was performed in 2-s cycle time data-dependent mode by higher-energy collisional dissociation (or beam-type collision induced dissociation) with a precursor window of 1.6 *m*/*z* and a normalized collision energy of 30.0; MS2 spectra were recorded in the Orbitrap at a resolution of 30,000. Singly charged precursors were excluded from fragmentation, and the dynamic exclusion was set to 60 s.

For data analysis, Data-Dependent Acquisition raw data files were analyzed using the MaxQuant software suite (version 2.0.3.0, www.maxquant.org)[65] for the identification and relative quantification of proteins. 'Match between runs' was disabled, and a false discovery rate of 0.01 for peptides and proteins and a minimum peptide length of 6 amino acids were required. The Andromeda search engine was used to search the MS/MS spectra against the *Danio rerio* UniProt database (version March 2022) concatenated with the reversed versions of all sequences and a contaminant database listing typical background proteins. A maximum of two missed cleavages was allowed. MS/MS spectra were analyzed using MaxQuant's default settings for Orbitrap and ion trap spectra. The maximum precursor ion charge state used for searching was 7, and the enzyme specificity was set to trypsin. Further modifications were cysteine carbamidomethylation (fixed) as well as methionine oxidation (variable). The minimum number of peptides for positive protein identification was set to 2. The minimum number of razor and unique peptides was set to 1. Only unique and razor peptides—unmodified, with oxidized methionine, or N-terminally acetylated—were used for protein quantitation. The minimal score for modified peptides was set to 40 (default value).

SORT sequencing. For scRNA-seq, cells were prepared as described above and sorted into 384-well plates. Plates were processed by Single Cell Discoveries using the SORT-seq protocol[66]. Illumina sequencing libraries were prepared using TruSeq Small RNA primers (Illumina) and paired-end sequenced with a read length of 75 bp on the Illumina NextSeq platform. In total, ten 384-well plates were sequenced containing one cell per well, two plates per cell type (bMΦs, macrophages, neutrophils from WT and bMΦs and metaphocytes from *csf1ra*$^{-/-}$*b*$^{-/-}$) Mapping was performed against the zebrafish reference genome assembly version 9 (Zv9). Next, single-cell data were analyzed using Seurat[67]. The following parameters were used: variable features = all genes, dimensions = 50 and resolution = 0.2. This resulted in the identification of ten clusters that were plotted in a two-dimensional Uniform Manifold Approximation and Projection (UMAP).

Statistical analysis and experimental setup

For each in vivo experiment, animals from the same clutch were divided into different treatment groups without any bias. The whole clutch was excluded if more than 10% of control embryos displayed obvious developmental defects. Animals were randomly selected for analysis and imaging, and, if applicable, genotyped afterward. If necessary, statistical analysis was performed using SPSS 20 (IBM). To compare two groups, statistical analysis was performed using a Kruskal–Wallis test followed by Dunn's multiple comparisons test versus WT. For multiple groups, statistical analysis was performed using a Kruskal–Wallis test followed by Dunn's multiple comparisons test versus WT.

Ethics declarations
We have complied with all relevant ethical regulations.

Reporting summary
Further information on research design is available in the Nature Portfolio Reporting Summary linked to this article.

Data availability
Mass spectrometry raw data files were uploaded to the ProteomeXchange Consortium via the PRIDE partner repository with the data identifier PXD052344. The scRNA-seq dataset has been deposited at the NCBI Gene Expression Omnibus (GEO) repository under accession number GSE296640. Source data are provided with this paper.

References

50. Wakayama, Y., Fukuhara, S., Ando, K., Matsuda, M. & Mochizuki, N. Cdc42 mediates Bmp-induced sprouting angiogenesis through Fmnl3-driven assembly of endothelial filopodia in zebrafish. *Dev. Cell* **32**, 109–122 (2015).
51. Ganis, J. J. et al. Zebrafish globin switching occurs in two developmental stages and is controlled by the LCR. *Dev. Biol.* **366**, 185–194 (2012).
52. Helker, C. S. M. et al. The zebrafish common cardinal veins develop by a novel mechanism: lumen ensheathment. *Development* **140**, 2776–2786 (2013).
53. Lin, H.-F. et al. Analysis of thrombocyte development in CD41–GFP transgenic zebrafish. *Blood* **106**, 3803–3810 (2005).
54. Patterson, L. B. & Parichy, D. M. Interactions with iridophores and the tissue environment required for patterning melanophores and xanthophores during zebrafish adult pigment stripe formation. *PLoS Genet.* **9**, e1003561 (2013).
55. Oosterhof, N. et al. Homozygous mutations in CSF1R cause a pediatric-onset leukoencephalopathy and can result in congenital absence of microglia. *Am. J. Hum. Genet.* **104**, 936–947 (2019).
56. Tian, Y. et al. The first wave of T lymphopoiesis in zebrafish arises from aorta endothelium independent of hematopoietic stem cells. *J. Exp. Med.* **214**, 3347–3360 (2017).
57. Davison, J. M. et al. Transactivation from Gal4-VP16 transgenic insertions for tissue-specific cell labeling and ablation in zebrafish. *Dev. Biol.* **304**, 811–824 (2007).
58. Beis, D. et al. Genetic and cellular analyses of zebrafish atrioventricular cushion and valve development. *Development* **132**, 4193–4204 (2005).
59. Gering, M. & Patient, R. Hedgehog signaling is required for adult blood stem cell formation in zebrafish embryos. *Dev. Cell* **8**, 389–400 (2005).
60. Zang, L., Shimada, Y., Nishimura, Y., Tanaka, T. & Nishimura, N. Repeated blood collection for blood tests in adult zebrafish. *J. Vis. Exp.* **30**, e53272 (2015).
61. Pugach, E. K., Li, P., White, R. & Zon, L. Retro-orbital injection in adult zebrafish. *J. Vis. Exp.* https://doi.org/10.3791/1645 (2009).
62. Gombash Lampe, S. E., Kaspar, B. K. & Foust, K. D. Intravenous injections in neonatal mice. *J. Vis. Exp.* **11**, e52037 (2014).
63. Akitake, C. M., Macurak, M., Halpern, M. E. & Goll, M. G. Transgenerational analysis of transcriptional silencing in zebrafish. *Dev. Biol.* **352**, 191–201 (2011).
64. Weijts, B., Tkachenko, E., Traver, D. & Groisman, A. A four-well dish for high-resolution longitudinal imaging of the tail and posterior trunk of larval zebrafish. *Zebrafish* **14**, 489–491 (2017).
65. Tyanova, S., Temu, T. & Cox, J. The MaxQuant computational platform for mass spectrometry-based shotgun proteomics. *Nat. Protoc.* **11**, 2301–2319 (2016).
66. Muraro, M. J. et al. A single-cell transcriptome atlas of the human pancreas. *Cell Syst.* **3**, 385–394 (2016).
67. Hao, Y. et al. Integrated analysis of multimodal single-cell data. *Cell* **184**, 3573–3587 (2021).

Acknowledgements
We thank the present and past lab members for helpful discussions and technical help. We thank T. van van Ham (Erasmus MC), S. Schulte-Merker (University of Münster), A. Meijer (Leiden University) and D. Traver (Cedars-Sinai Medical Center) for sending zebrafish lines. We thank the Hubrecht Institute's Animal Facility, Hubrecht Imaging Center and FACS facility for support. This work received support from a Landsteiner Foundation for Blood Transplantation Research (LSBR 22860; B.W.), a KWF Dutch Cancer Society (13549; C.R.), and an NWO Dutch Research Council (OCENW.M20.178; C.R.). We thank G. Kops (Hubrecht Institute), J. Bakkers (Hubrecht Institute), J. Bothma (Hubrecht Institute) and E. Wehrens (Princess Máxima Center for Pediatric Oncology) for critical review of the paper.

Author contributions
B.W. initiated the project. C.R. and B.W. designed experiments, performed data analysis and formatted all figures and videos. B.W. performed all the biological experiments on zebrafish, and C.R. and B.W. performed all the biological experiments on mice. J.A.A.D. performed proteomic experiments and data analysis, with the help of B.W and C.R. B.W. performed scRNA-seq data analysis with the help of C.R. C.R. and B.W. wrote the paper, prepared all figures and edited all videos. All authors read and approved the final paper.

Competing interests
The authors declare no competing interests.

Additional information
Extended data is available for this paper at https://doi.org/10.1038/s41590-026-02481-y.

Supplementary information The online version contains supplementary material available at https://doi.org/10.1038/s41590-026-02481-y.

Correspondence and requests for materials should be addressed to Bart Weijts or Catherine Robin.

Peer review information *Nature Immunology* thanks the anonymous reviewer(s) for their contribution to the peer review of this work. Primary Handling Editor: S. Houston, in collaboration with the *Nature Immunology* team.

https://doi.org/10.1038/s41590-026-02481-y

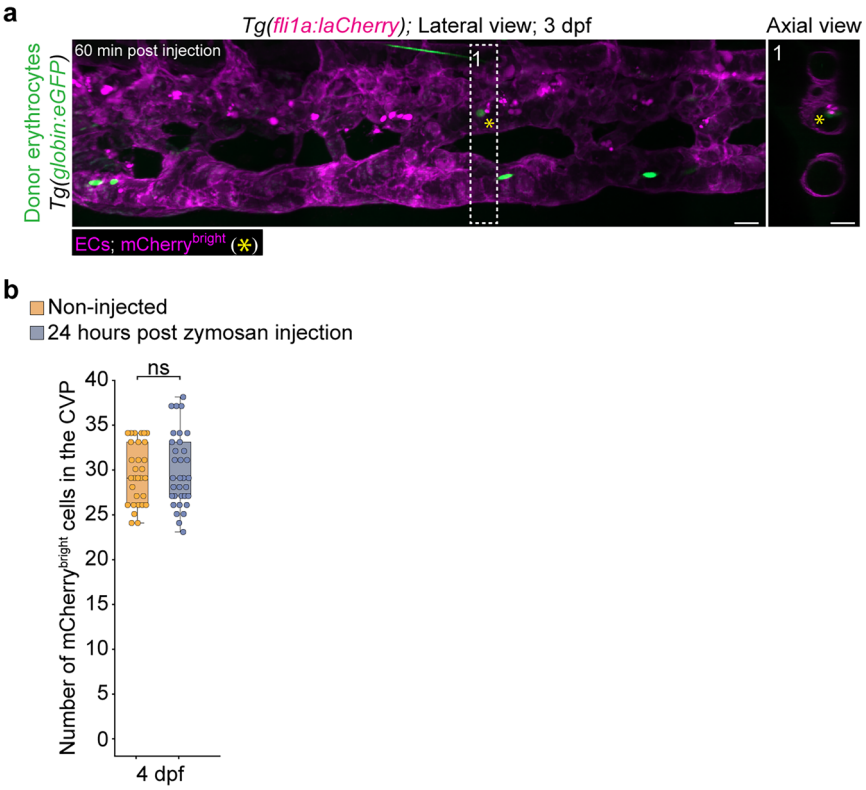

Extended Data Fig. 1 | Intravascular phagocytosis of donor erythrocytes by fli1a mCherry^{bright} cells. a, Images of the CVP of a 3 dpf *Tg(fli1a:laCherry)* embryo 60 minutes after the intravascular injection of fluorescently labelled donor erythrocytes (*globin:eGFP*$^{+}$, green). mCherry^{bright} cell in dashed box (asterisk). Lateral and axial views are shown. **b**, Quantification of mCherry^{bright} cells in the CVP region in non-injected embryos or 24 hours post intravascular injection of zymosan. Images are representative of n = 1 (5 embryos) (**a**). n = 1, non-injected (30 embryos); zymosan injected (33 embryos) (**b**). Scale bars: 20 µm. CVP, caudal vein plexus. Box plot shows the median (center), first and third quartiles (bounds) and 1.5 times the interquartile range (whiskers) (**b**). Statistical analysis was performed using a two-tailed Mann–Whitney U test for comparison of two conditions (**b**).

https://doi.org/10.1038/s41590-026-02481-y

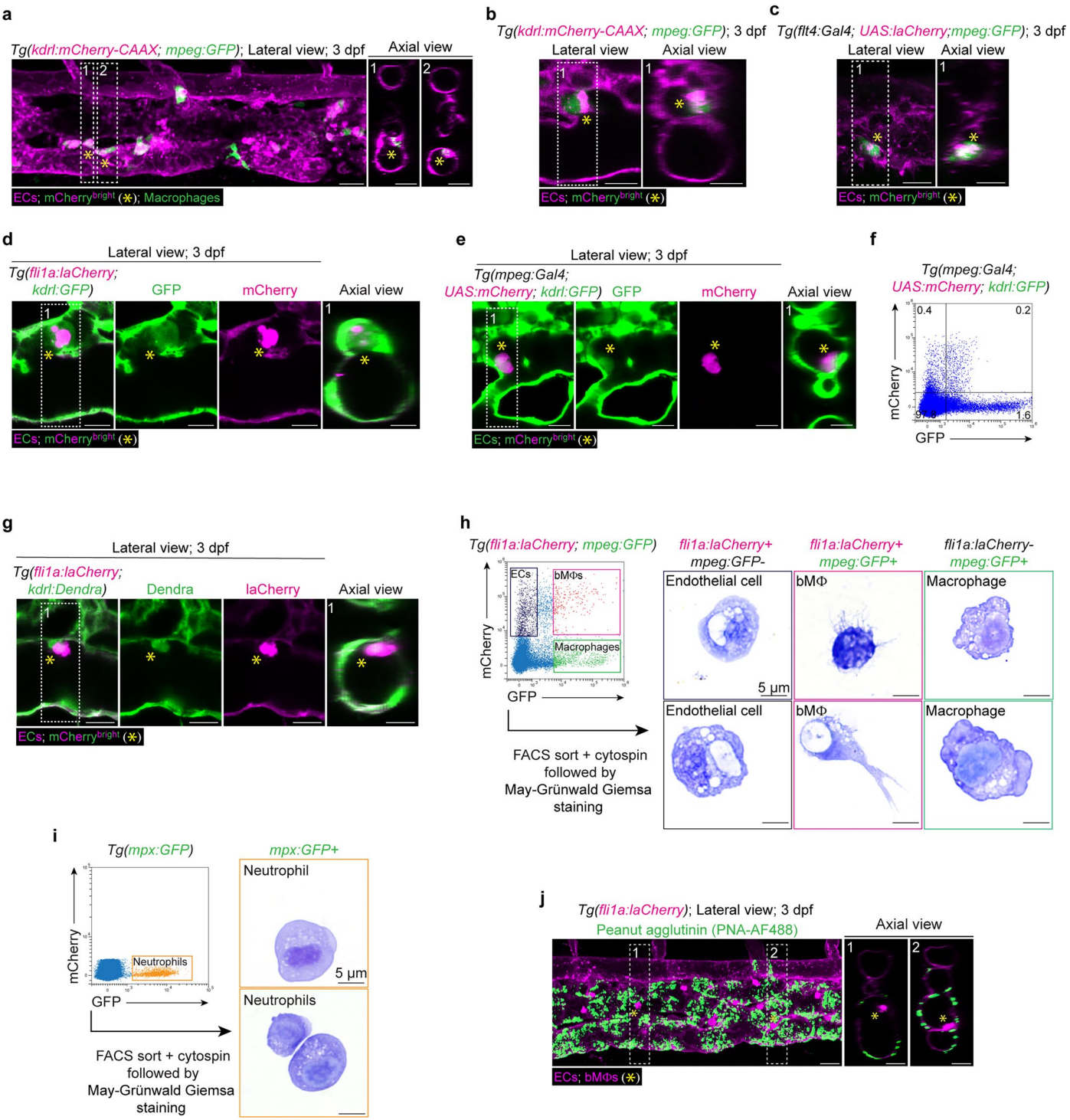

Extended Data Fig. 2 | Phenotypic and functional characterization of bMΦs. a-e, Images and close-up of the CVP region of 3 dpf embryos from (**a, b**) *Tg(kdrl:mCherry-CAAX;mpeg:GFP)*, where all ECs are labelled with mCherry-CAAX (*kdrl*) and macrophages with GFP (*mpeg*), (**c**) *Tg(flt4:Gal4;UAS:laCherry; mpeg:GFP)*, where all ECs are labelled with laCherry (*flt4*) and macrophages with GFP (*mpeg*), (**d**) *Tg(fli1a:laCherry;kdrl:GFP)*, where all ECs are labelled with laCherry (*fli1a*) and GFP (*kdrl*) and (**e**) *Tg(mpeg:Gal4;UAS:mCherry;kdrl:GFP)*, where all ECs are labelled with GFP (*kdrl*) and macrophages with mCherry (*mpeg*). Asterisks show mCherry^{+}GFP^{+} cells. **f**, Representative flow cytometry plot of 3 dpf *Tg(mpeg:Gal4;UAS:mCherry;kdrl:GFP)* embryos. **g**, Close-up of the CVP region of a 3 dpf *Tg(fli1a:laCherry;kdrl:Dendra)* embryo, where all ECs are labelled with laCherry (*fli1a*) and Dendra (green; *kdrl*). Asterisks show mCherry^{+}GFP^{+} cell. **h, i**, Representative flow cytometry plots and gating strategy for sorting the indicated cell populations. Sorted cells were cytocentrifuged (cytospin) and stained by May-Grünwald Giemsa before imaging. Representative pictures of ECs, bMΦs, tissue macrophages (**h**) and neutrophils (**i**) sorted based on the indicated fluorophores. **j**, Images of the CVP of a 3 dpf *Tg(fli1a:laCherry)* embryo intravascularly injected with fluorescently labelled PNA (PNA-AF488, green). PNA is a plant lectin protein that recognizes the galactose β (1 - > 3) N-acetyl galactosamine carbohydrate sequence. bMΦs are depicted by asterisks. Images are representative of n = 3 independent experiments (30 embryos) (**a-g**), n = 1 (10 embryos) (**j**). Sort and cytospin were performed on clutches of different families from n = 3 independent experiments (**h, i**). Scale bars: 20 µm (**a-e, g, j**), 5 µm (**h, i**). CVP, caudal vein plexus; EC, endothelial cell; PNA, peanut agglutinin; bMΦ, blood vessel-resident macrophage.

https://doi.org/10.1038/s41590-026-02481-y

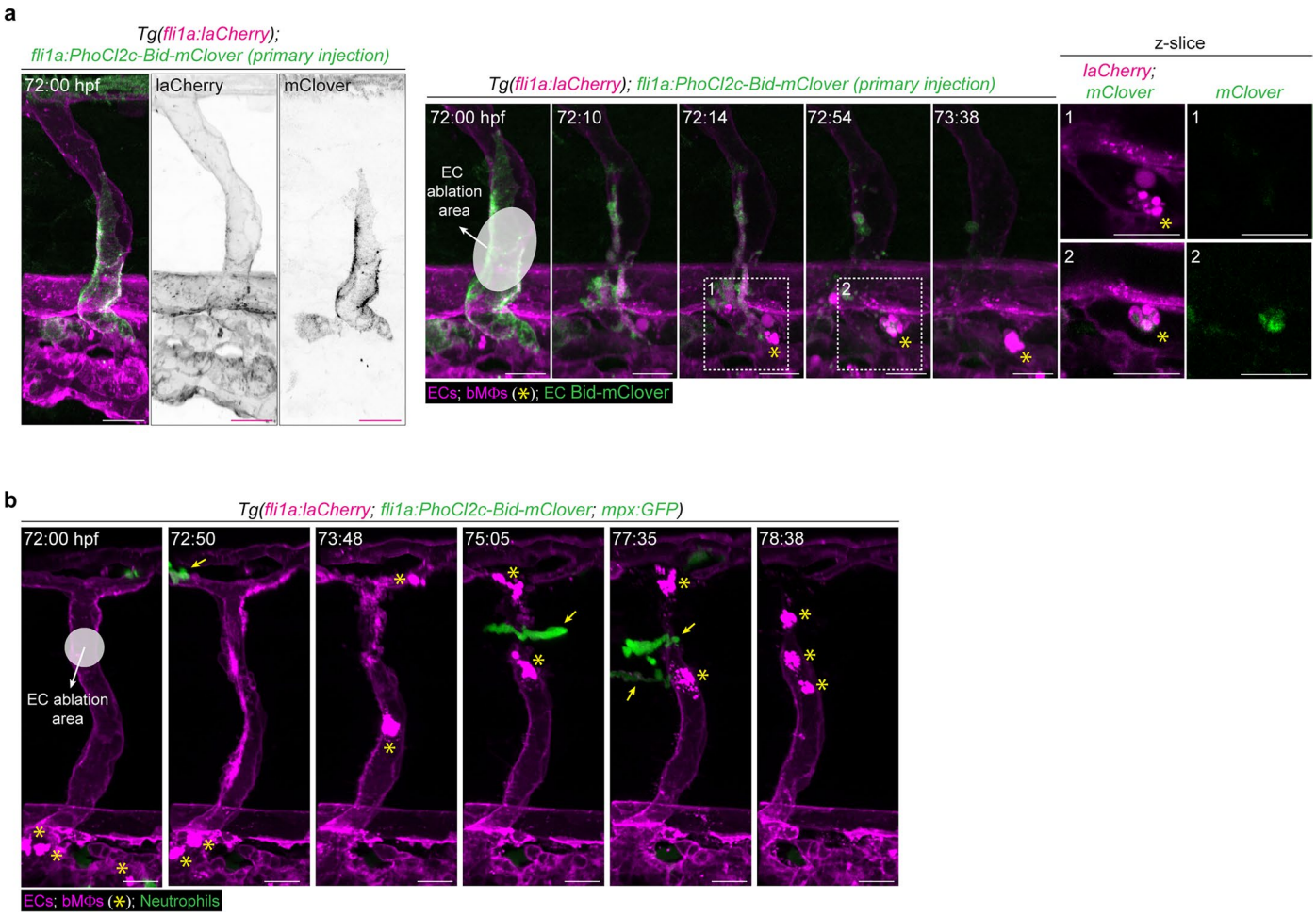

Extended Data Fig. 3 | bMΦs respond to vascular damage. a, Still images of Supplementary Video 12 in which the *fli1a:PhoCl2c-Bid-mClover* construct was injected in the single cell stage (referred to as primary injection) for mosaic expression in ECs. Targeting area is indicated by the translucent circle. ECs are laCherry$^+$ and either negative or positive for GFP. bMΦ is laCherry$^+$GFP$^-$ before and laCherry$^+$GFP$^+$ after debris phagocytosis, respectively (asterisk). **b**, Still images of Supplementary Video 13 in which ECs of an ISV have been optogenetically ablated in a 3 dpf *Tg(fli1a:laCherry;fli1a:PhoCl2c-Bid-mClover;mpx:GFP)* embryo (see scheme top panel in Fig. 3f). Targeting area is indicated by the translucent circle, ECs are laCherry$^+$GFP$^-$, bMΦs are laCherry$^+$GFP$^+$ (asterisks) and neutrophils are mCherry$^-$GFP$^+$ (yellow arrows). Scale bars: 20 µm. Images are representative of n = 3 independent time-lapse experiments. EC, endothelial cell; bMΦ, blood vessel-resident macrophage.

https://doi.org/10.1038/s41590-026-02481-y

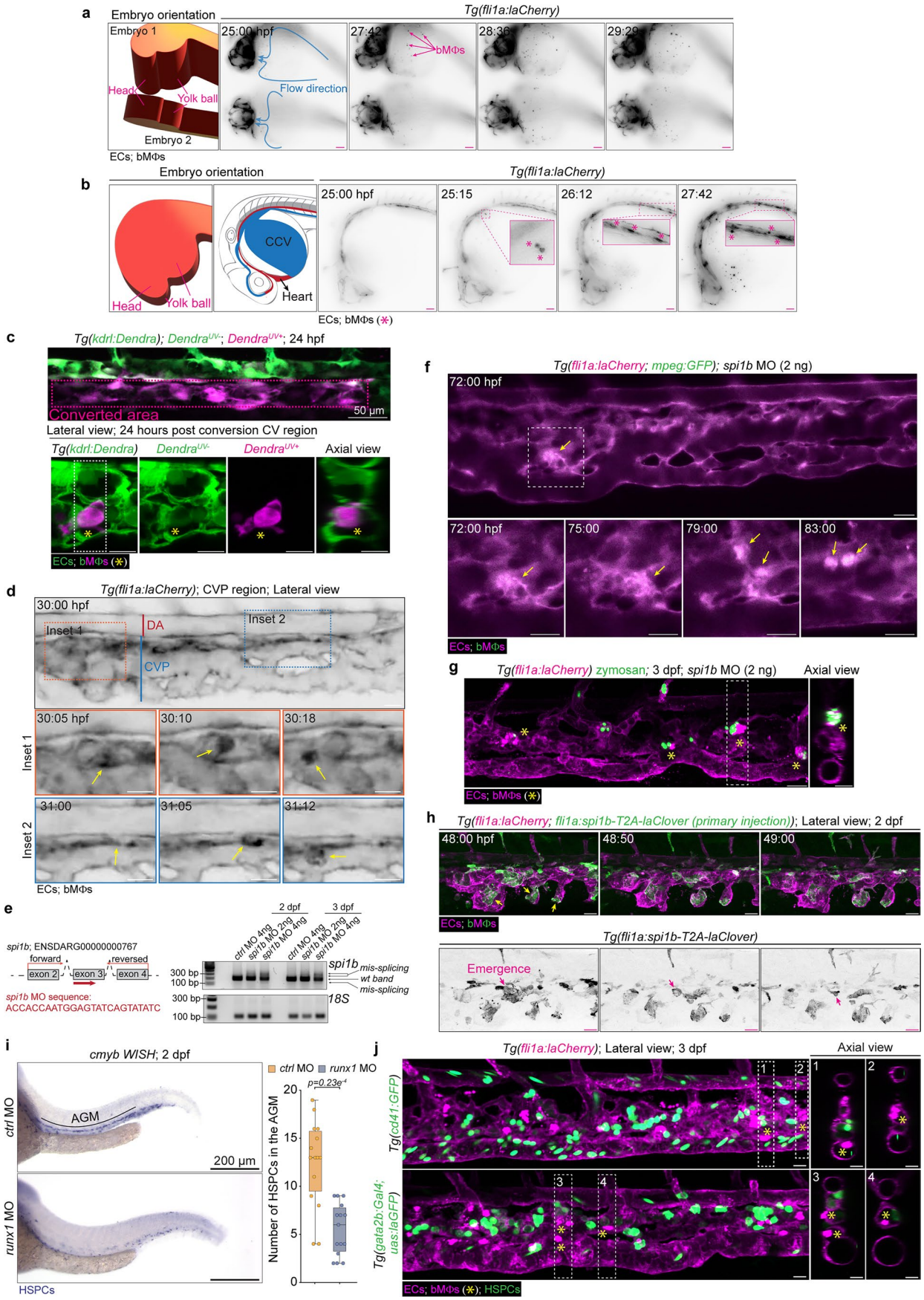

Extended Data Fig. 4 | See next page for caption.

https://doi.org/10.1038/s41590-026-02481-y

Extended Data Fig. 4 | Endothelial origin of bMΦs. a, Time-lapse still images of *Tg(fli1a:laCherry)* embryos, with the left panels depicting in schemes the embryo orientation as mounted for imaging. Blue arrows indicate blood flow direction through the CCV that runs bi-laterally over the yolk ball. Magenta arrows show bMΦs. **b**, Time-lapse still images of a *Tg(fli1a:laCherry)* embryo, with the two most left panels depicting in schemes the embryo orientation. Insets are a magnification of dashed boxes, showing the emergence of bMΦs (asterisks). **c**, PCV region of a 3 dpf *Tg(kdrl:Dendra)* embryo (top panel). Region exposed to UV light to photoconvert cells from green to red is marked with dashed box. CV region one day post conversion (lower panel). All ECs are labelled with Dendra (green; *kdrl*). Asterisk shows a cell with a macrophage morphology (magenta) photoconverted in the PCV and located 24 h later in the CV region. **d**, Still images of Supplementary Video 15, showing the transition of venous ECs into bMΦs through EMacT (yellow arrows). Lower panels are a magnification of the orange and blue dashed boxes. **e**, Schematic drawing of the partial exon-intron region of the *spi1b* gene and MO targeting site (thick red arrow), including the forward and reversed primers used for PCR (orange arrows). Image of agarose gel showing the mis-splicing of the *spi1b* gene. **f**, Time-lapse still images of the CVP of a 3 dpf *Tg(fli1a:laCherry; mpeg:GFP)* embryo after low dose *spi1b* MO (2 ng) injection, showing the *de novo* emergence of bMΦs (arrows). **g**, Image of *Tg(fli1a:laCherry) spi1b* low dose morphants injected with zymosan (green) at 3 dpf. Asterisks indicate *de novo* generated bMΦs (mCherry^{bright}) that phagocytosed zymosan. **h**, Time-lapse still images of a 2 dpf *Tg(fli1a:laCherry; fli1a:spi1b-T2A-laClover)* embryo in which *spi1b-T2A-laClover* is mosaically over-expressed in ECs of the CVP. Yellow arrows (top panels) indicate ECs ectopically expressing *spi1b*. Magenta arrows (lower panels) follow the emergence of a bMΦ directly from an EC embedded in the blood vessel wall (single GFP channel shown). **i**, Left, WISH of the HSPC marker *cmyb* performed on *ctrl* MO and *runx1* MO injected embryos. Right panel, quantification of HSPCs (*cmyb*$^{+}$) in the AGM region of *ctrl* and *runx1* morphants. **j**, Images of the CVP of 3 dpf *Tg(fli1a:laCherry; cd41:GFP)* (top panels) and *Tg(fli1a:laCherry; gata2b:KalTA4; uas:laGFP)* (bottom panels) embryos in which HSPCs are GFP^{+} (*cd41* or *gata2b*) and bMΦs are mCherry^{bright} (*fli1a*, asterisks). Images are representative of n = 3 independent time-lapse experiments (**a, b, d, f, h**), n = 1 (10 embryos) (**c**), n = 5 embryos per time point and condition (**e**); n = 2 (10 embryos) (**g**), n = 1 (15 embryos/condition) (**i**), n = 3 (30 embryos) (**j**). Scale bars: 20 µm. CCV, common cardinal vein; bMΦ, blood vessel-resident macrophage; WB, western blot; WISH, whole mount *in situ* hybridization; MO, morpholino oligonucleotide; EC, endothelial cell; CVP, caudal vein plexus; PCV, posterior cardinal vein; AGM, aorta-gonad-mesonephros region. Box plot shows the median (center), first and third quartiles (bounds) and 1.5 times the interquartile range (whiskers) (**i**). Statistical analysis was performed using a two-tailed Mann–Whitney U test for comparison of two conditions (**i**).

https://doi.org/10.1038/s41590-026-02481-y

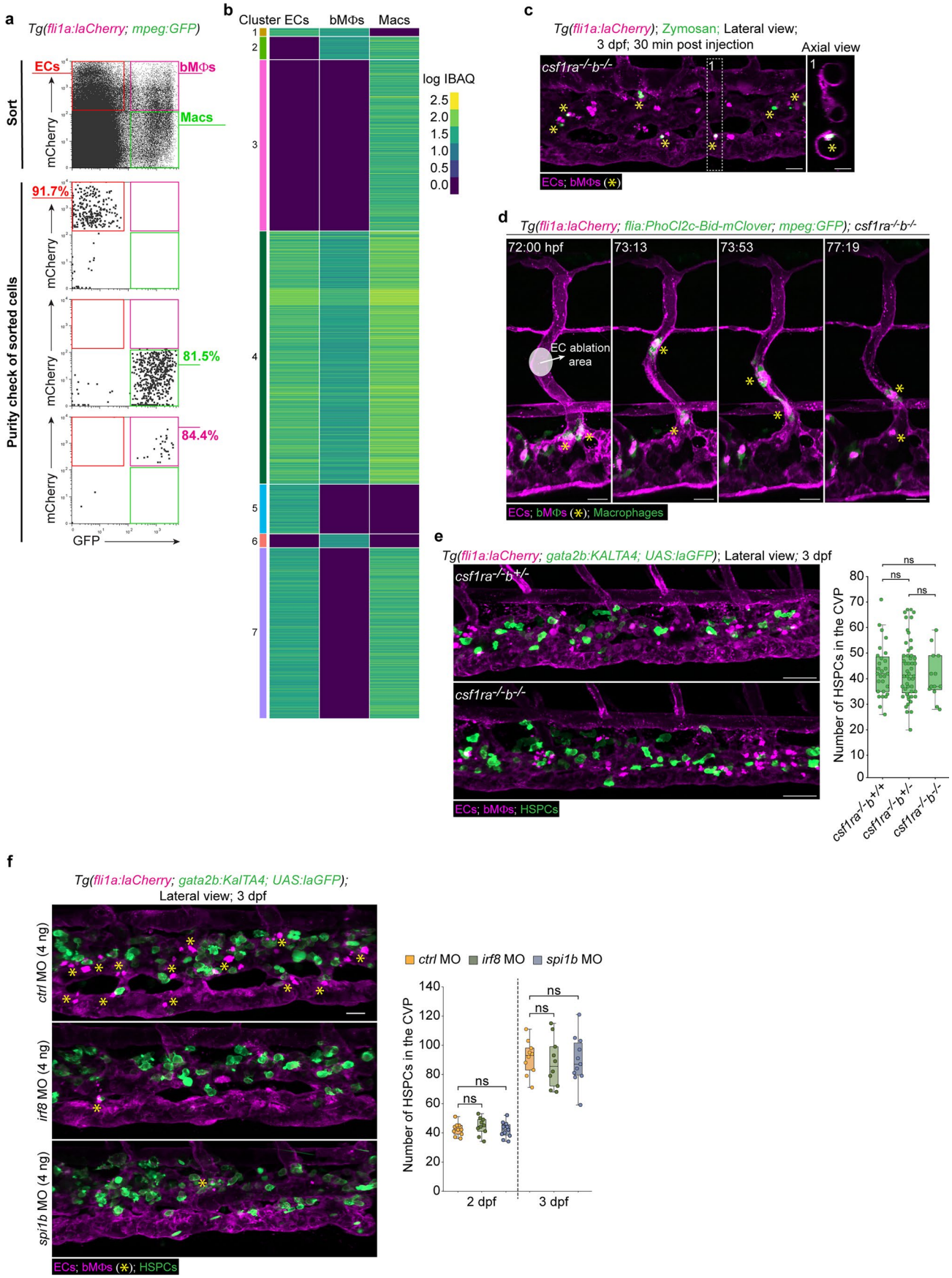

Extended Data Fig. 5 | See next page for caption.

https://doi.org/10.1038/s41590-026-02481-y

Extended Data Fig. 5 | Gating strategy, mass spectrometry analysis, and functionality of *csf1r* deficient bMΦs. a, Representative flow cytometry plot (top) and gating strategy for sorting the indicated cell populations for mass spectrometry. Plots (bottom) showing the purity of the sorted cell populations gated in (**a**). **b**, Heatmap of the clustered proteins as shown in Fig. 5b. **c**, Image of the CVP of a 3 dpf *Tg(fli1a:laCherry) csf1ra*$^{-/-}$*b*$^{-/-}$ (double mutant) embryo after intravascular injection of fluorescently labelled zymosan (green). Injection in the CCV as indicated in scheme in Fig. 1a. Asterisks indicate bMΦs that have phagocytosed zymosan particles. **d**, Still images of Supplementary Video 17 showing the optogenetic ablation of ECs in an ISV of a 3 dpf *Tg(fli1a:laCherry; fli1a:PhoCl2c-Bid-mClover; mpeg:GFP) csf1ra*$^{-/-}$*b*$^{-/-}$ (double mutant) embryo (see scheme top panel in Fig. 3f). Targeting area is indicated by the translucent circle. ECs are GFP^{-}laCherry^{+} and bMΦs are GFP^{+}laCherry^{+} (asterisks). **e**, Images and quantification of HSPCs in the CVP region at 3 dpf in *Tg(fli1a:laCherry; gata2b:KalTA4; uas:laGFP) csf1ra*$^{-/-}$*b*$^{+/-}$ (top panel) and *csf1ra*$^{-/-}$*b*$^{-/-}$ (double mutant, bottom panel) embryos. **f**, Images and quantification of HSPCs in the CVP region at 3 dpf of *Tg(fli1a:laCherry; gata2b:KalTA4; UAS:laGFP)* embryos injected with *ctrl, irf8 or spi1b* MO. Images are representative of n = 5 independent experiments (5 embryos) (**c, d**), quantification n = 1 (89 embryos (**e**); 10 embryos/condition (**f**)). Scale bars: 20 µm. dpf, days post fertilisation; EC, endothelial cell; Macs, tissue macrophages; PCV, posterior cardinal vein; CCV, common cardinal vein; ISV, intersegmental vessel; ns, not significant. Box plots show the median (center), first and third quartiles (bounds) and 1.5 times the interquartile range (whiskers) (**e, f**). Statistical analysis was performed using a Kruskal–Wallis test followed by Dunn's multiple comparisons test versus WT (**e, f**).

https://doi.org/10.1038/s41590-026-02481-y

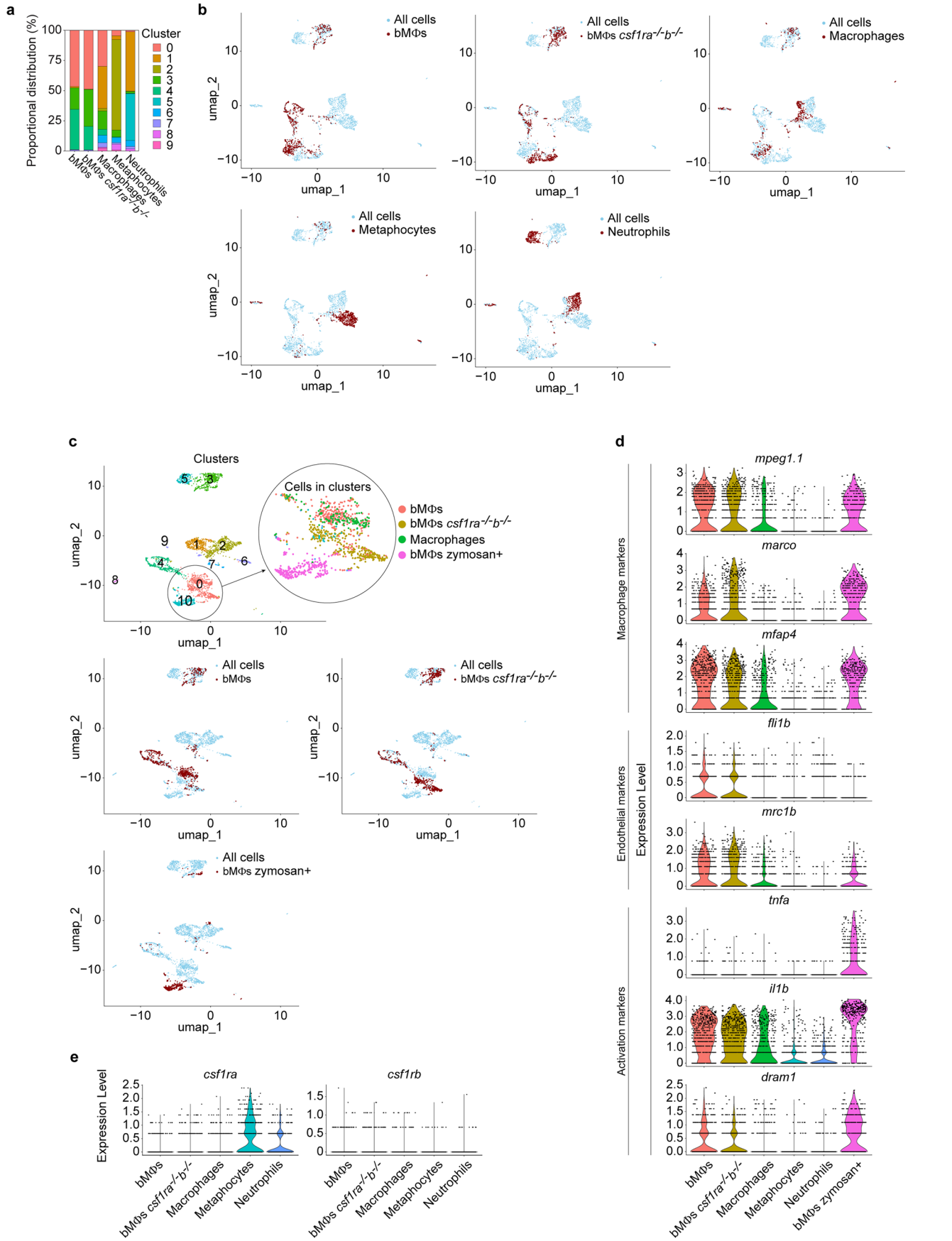

Extended Data Fig. 6 | scRNA-sequencing analysis of bMΦs. a, Distribution of the indicated sorted cell-types in the different scRNA-seq clusters. **b**, Projection of the different sorted cell populations on the UMAP scatter plots. **c**, UMAP scatter plots after the addition of bMΦs sorted from zymosan injected embryos (bMΦs zymosan^{+}) scRNA-seq data shown in Fig. 5f. **d**, Violin plots of gene expression levels in the indicated cell populations. **e**, Violin plots of gene expression levels of *csf1r* genes in the indicated cell populations.

https://doi.org/10.1038/s41590-026-02481-y

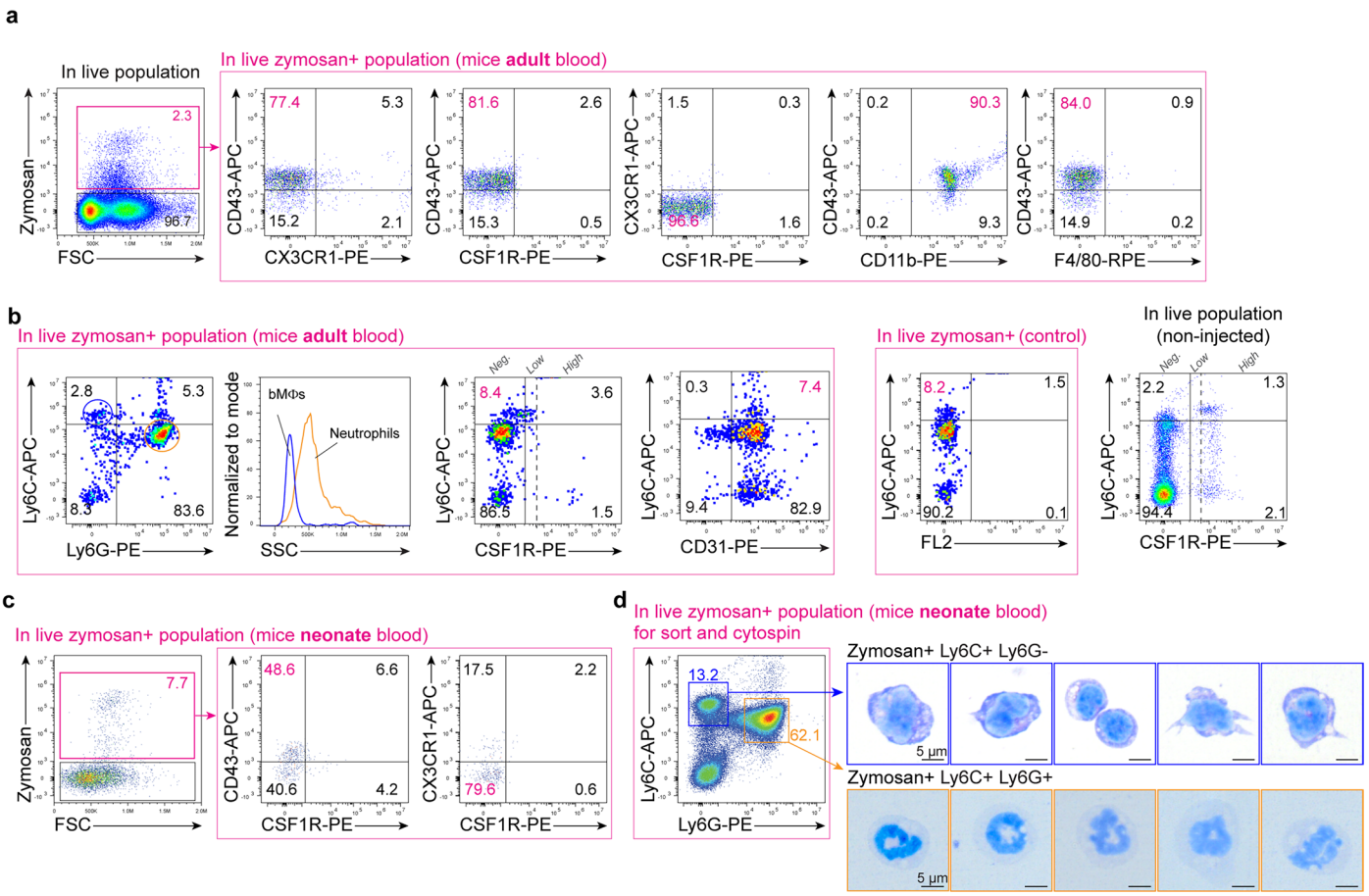

Extended Data Fig. 7 | bMΦs in adult and neonatal mice. a, Representative flow cytometry plots of cells that phagocytosed zymosan in the bloodstream of adult mice (zymosan$^+$ cells in magenta gate are CD43$^+$ CSF1R$^-$ CX3CR1$^-$ CD11b$^+$ F4/80$^-$). **b**, Representative flow cytometry plots and histogram of two main populations of cells that phagocytosed zymosan in the bloodstream of adult mice; bMΦs (zymosan$^+$ Ly6C$^+$ Ly6G$^-$ SSC^{low} CSF1R$^{-/low}$ CD31$^+$) and neutrophils (zymosan$^+$ Ly6C$^+$ Ly6G$^+$ SSC^{high} CSF1R$^-$). Two most right panels are controls for gating strategy. **c**, Representative flow cytometry plots of cells that phagocytosed zymosan in the bloodstream of neonatal mice (zymosan$^+$ cells in magenta gate are CD43$^+$ CSF1R$^-$ CX3CR1$^-$). **d**, Representative flow cytometry plot and gating strategy for sorting zymosan phagocytosing cells (bMΦs [zymosan$^+$ Ly6C$^+$ Ly6G$^-$] and neutrophils [zymosan$^+$ Ly6C$^+$ Ly6G$^+$]) from the bloodstream of neonatal mice. Sorted cells were cytocentrifuged (cytospin) and stained by May-Grünwald Giemsa before imaging. Representative pictures of bMΦs (top panels) and neutrophils (bottom panels) are shown. Flow cytometry plots are representative of n = 3 (3 injected and 2 non-injected adults/n; 6 injected neonates/n) independent experiments (**a**-**d**). Percentages of populations are indicated in the quadrants and gates of each plot.

https://doi.org/10.1038/s41590-026-02481-y

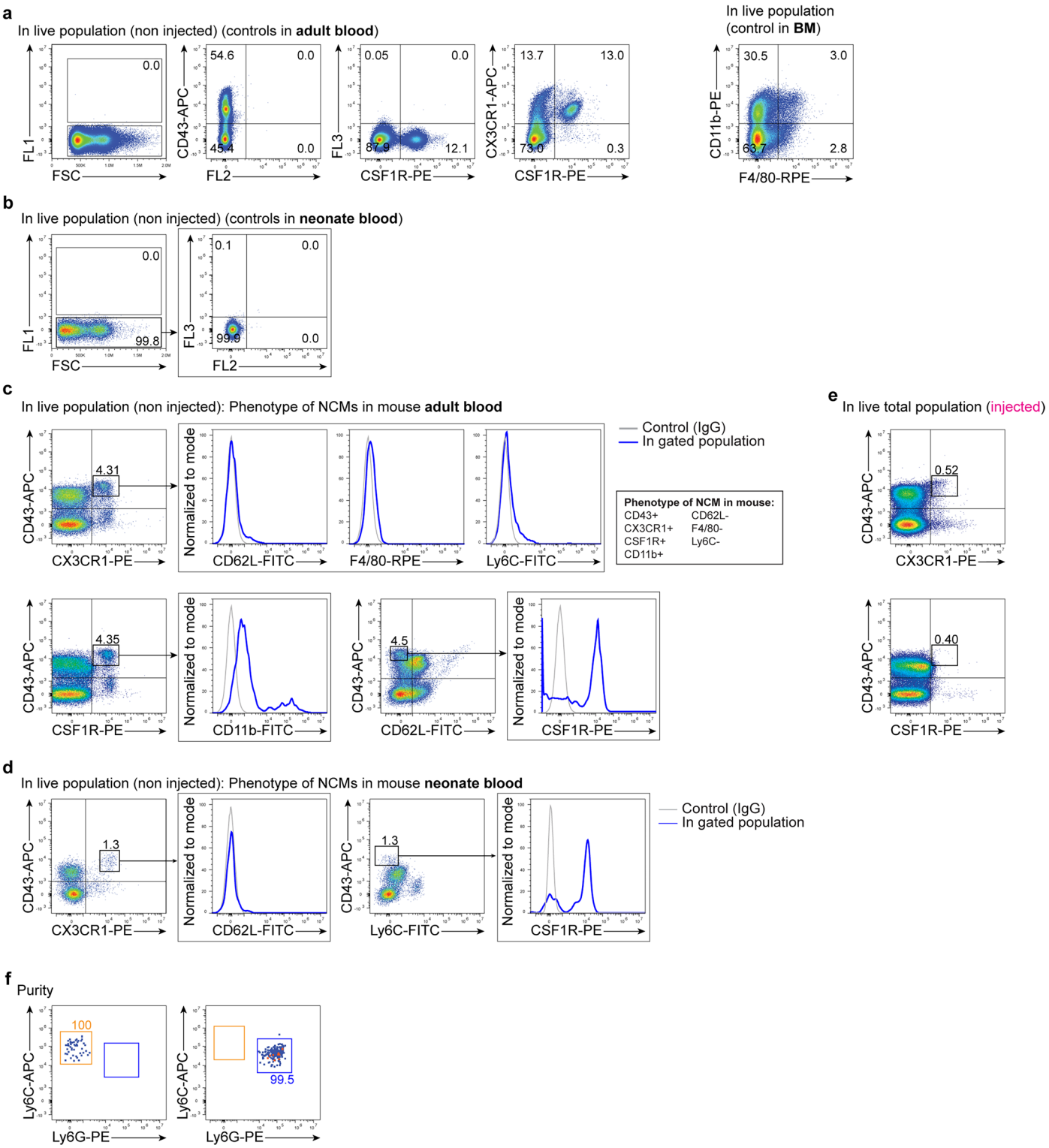

Extended Data Fig. 8 | Flow cytometry controls for the analysis of bMΦs in adult and neonatal mice. a, Representative flow cytometry control plots on blood and bone marrow of adult mice. **b** Representative flow cytometry control plots on neonatal blood. **c**, Representative flow cytometry plots showing the phenotype of patrolling/non-classical monocytes (NCMs) in the blood of adult mice ($CD43^+$ $CX3CR1^+$ $CSF1R^+$ $CD11b^+$ $CD62L^-$ $F4/80^-$ $Ly6C^-$). **d**, Representative flow cytometry showing the phenotype of NCM in the blood of neonatal mice ($CD43^+$ $CX3CR1^+$ $CD62L^-$ $CSF1R^+$ $Ly6C^-$). **e**, Representative flow cytometry plots of the few NCMs remaining in the blood of adult mice intravenously injected with zymosan. **f**, Purity check after sorting of bMΦs ($Ly6C^+Ly6G^-$) and neutrophils ($Ly6C^+Ly6G^+$) shown in Extended Data Fig. 7d. Flow cytometry plots are representative of n = 3 (3 injected and 2 non-injected adults/n; 2 non-injected neonates/n) independent experiments (**a**-**f**). Percentages of populations are indicated in the gates and quadrants of each plot. BM, bone marrow.

nature portfolio

Corresponding author(s): Robin, Weijts

Last updated by author(s): Feb 25, 2026

Reporting Summary

Nature Portfolio wishes to improve the reproducibility of the work that we publish. This form provides structure for consistency and transparency in reporting. For further information on Nature Portfolio policies, see our Editorial Policies and the Editorial Policy Checklist.

Statistics

For all statistical analyses, confirm that the following items are present in the figure legend, table legend, main text, or Methods section.

n/a	Confirmed
☐	☒ The exact sample size (*n*) for each experimental group/condition, given as a discrete number and unit of measurement
☐	☒ A statement on whether measurements were taken from distinct samples or whether the same sample was measured repeatedly
☐	☒ The statistical test(s) used AND whether they are one- or two-sided *Only common tests should be described solely by name; describe more complex techniques in the Methods section.*
☒	☐ A description of all covariates tested
☐	☒ A description of any assumptions or corrections, such as tests of normality and adjustment for multiple comparisons
☐	☒ A full description of the statistical parameters including central tendency (e.g. means) or other basic estimates (e.g. regression coefficient) AND variation (e.g. standard deviation) or associated estimates of uncertainty (e.g. confidence intervals)
☐	☒ For null hypothesis testing, the test statistic (e.g. *F*, *t*, *r*) with confidence intervals, effect sizes, degrees of freedom and *P* value noted *Give P values as exact values whenever suitable.*
☒	☐ For Bayesian analysis, information on the choice of priors and Markov chain Monte Carlo settings
☒	☐ For hierarchical and complex designs, identification of the appropriate level for tests and full reporting of outcomes
☒	☐ Estimates of effect sizes (e.g. Cohen's *d*, Pearson's *r*), indicating how they were calculated

Our web collection on statistics for biologists contains articles on many of the points above.

Software and code

Policy information about availability of computer code

Data collection	FlowJo X; ; R Software 3.1.1 (2014-07-10) (R Core Team, 2013); Zeiss ZEN system; Leica LAS X software to capture images;
Data analysis	Zeiss ZEN system, Leica LAS X, FIJI (MultiStackReg to correct for drift), Imaris, Imaris Sticher (for stiching images), Adobe Illustrator and After Effects, MaxQuant software, FlowJo X, Cytexpert

For manuscripts utilizing custom algorithms or software that are central to the research but not yet described in published literature, software must be made available to editors and reviewers. We strongly encourage code deposition in a community repository (e.g. GitHub). See the Nature Portfolio guidelines for submitting code & software for further information.

Data

Policy information about availability of data

All manuscripts must include a data availability statement. This statement should provide the following information, where applicable:

- Accession codes, unique identifiers, or web links for publicly available datasets
- A description of any restrictions on data availability
- For clinical datasets or third party data, please ensure that the statement adheres to our policy

MS raw data files were uploaded to the ProteomeXchange Consortium via the PRIDE partner repository with the data identifier PXD052344.
scRNA sequence were uploaded to the NCBI geo expression omnibus accession number XXXXX

Research involving human participants, their data, or biological material

Policy information about studies with human participants or human data. See also policy information about sex, gender (identity/presentation), and sexual orientation and race, ethnicity and racism.

Reporting on sex and gender	No research involving human participants
Reporting on race, ethnicity, or other socially relevant groupings	NA
Population characteristics	NA
Recruitment	NA
Ethics oversight	NA

Note that full information on the approval of the study protocol must also be provided in the manuscript.

Field-specific reporting

Please select the one below that is the best fit for your research. If you are not sure, read the appropriate sections before making your selection.

☒ Life sciences ☐ Behavioural & social sciences ☐ Ecological, evolutionary & environmental sciences

For a reference copy of the document with all sections, see nature.com/documents/nr-reporting-summary-flat.pdf

Life sciences study design

All studies must disclose on these points even when the disclosure is negative.

Sample size	Typically, we picked at least 20 animals randomly for each condition from a single clutch if quantification was needed. For time-lapse imaging, single embryos were imaged with high spatiotemporal resolution. For adults, we injected zymosna into 3 adult mice or zebrafish and used 2 uninjected adult animals as control.
Data exclusions	The whole clutch was excluded if more than 10% of untreated (control) embryos displayed obvious developmental defects.
Replication	Experiments were repeated in triplicate (different day, different breeding pair).
Randomization	Animals were randomly picked for analysis and imaging and if applicable genotyped afterwards
Blinding	Typically blinding was not performed as treated animals (chemically with Lat A or morphants) can be easily distinguished from untreated embryos due to their strong phenotype. Blinding was perform when quantifying mutant embryos and genotyped afterwards

Reporting for specific materials, systems and methods

We require information from authors about some types of materials, experimental systems and methods used in many studies. Here, indicate whether each material, system or method listed is relevant to your study. If you are not sure if a list item applies to your research, read the appropriate section before selecting a response.

Materials & experimental systems

n/a	Involved in the study
☐	☒ Antibodies
☒	☐ Eukaryotic cell lines
☒	☐ Palaeontology and archaeology
☐	☒ Animals and other organisms
☒	☐ Clinical data
☒	☐ Dual use research of concern
☒	☐ Plants

Methods

n/a	Involved in the study
☒	☐ ChIP-seq
☐	☒ Flow cytometry
☒	☐ MRI-based neuroimaging

Antibodies

Antibodies used	CD43-APC (BD Pharmingen; Cat#560663; Lot: 4115180; Clone: S7; 1:300) CX3CR1-PE (BD Pharmingen; Cat#567530; Lot: 1113444; Clone: Z8-50, 1:600)

CD31-PE (BD Pharmingen; Cat#553373; Lot:6014987; Clone: ME 13.3, 1:500)
Ly6C-FITC (BD Pharmingen; Cat#553104; Lot:33380; Clone: AL-21; 1:300)
CD11b-FITC (BD Pharmingen; Cat#553310; Lot:24571; Clone: M1/70, 1:600)
Ly-6C-APC (BD Pharmingen; Cat# 560595; Lot: 4099260; Clone:AL-21, 1:200)
Ly-6G-PE (BD Pharmingen; Cat# 561104; Lot: 4172280; Clone: 1A8, 1:200)
CD115-PE (CSF1R)(BD Pharmingen; Cat# 565249; Lot: 0336859; Clone: T38-320; 1:300)
CD62L-FITC (BD Pharmingen; Cat#553150; Lot: 30526; Clone:MEL-14, 1:1000)
CD11b-PE (BD Pharmingen; Cat#553311; Lot: 36540; Clone: M1/70, 1:600)
CX3CR1-APC (Biolegend; Cat#149007; Lot:B428612; Clone:SA011F11, 1:600)
F4/80-RPE (Bio-Rad; Cat# MCA497G; Clone: A3-1, 1:300)

Validation

Validation was performed by the manufacturer, as all antibodies are commercially available. All antibodies were nonetheless validated and titrated using mouse bone marrow cells expressing the receptor of interest. In addition, all antibodies employed here have been successfully used in mouse studies, as reported before (see vendor's information)

Animals and other research organisms

Policy information about studies involving animals; ARRIVE guidelines recommended for reporting animal research, and Sex and Gender in Research

Laboratory animals	All used zebrafish lines are listed in the Methods section and referenced according to the guidelines
Wild animals	The study did not involved wild animal
Reporting on sex	Sex determination occurs at later stages in zebrafish and is thus irrelevant for this study. For adult mice and zebrafish we used a near equal number of males and females
Field-collected samples	NA
Ethics oversight	All animal procedures performed at the Hubrecht Institute were approved by the local animal experiment committee and by the Animal Experimentation Committee (DEC) of the Royal Netherlands Academy of Arts and Sciences.

Note that full information on the approval of the study protocol must also be provided in the manuscript.

Plants

Seed stocks	NA
Novel plant genotypes	NA
Authentication	NA

Flow Cytometry

Plots

Confirm that:

☐ The axis labels state the marker and fluorochrome used (e.g. CD4-FITC).

☒ The axis scales are clearly visible. Include numbers along axes only for bottom left plot of group (a 'group' is an analysis of identical markers).

☐ All plots are contour plots with outliers or pseudocolor plots.

☒ A numerical value for number of cells or percentage (with statistics) is provided.

Methodology

Sample preparation	Embryonic tissues and embryos were collected from zebrafish according to standard procedure (see Methods for details). Blood collection for adult mice and fish, as well as neonates is descirbed in detail in the Methods
Instrument	Cytoflex SRT, BD Influx Cell Sorter
Software	Flow Jo X, Cytexpert

Cell population abundance	Purity was determined after sort after reanalysis of a cell sample.
Gating strategy	Cells were selected based on morphology (FSC/SSC), doublets exclusion, live/death staining (dapi) and positivity (gating strategy) was determined after examination of control zebrafish lines.

☒ Tick this box to confirm that a figure exemplifying the gating strategy is provided in the Supplementary Information.